The Thesis Committee for Evan Marley Hegarty certifies that this is the approved version of the following thesis:

Automated Parallel Immobilization Microfluidic Platforms for High-Throughput Neuronal Degeneration Studies with *C. elegans*

Committee:

Adela Ben-Yakar, Supervisor

Sudip Mondal

Automated Parallel Immobilization Microfluidic Platforms for High-Throughput Neuronal Degeneration Studies with *C. elegans*

by

Evan Marley Hegarty, B.S.M.E.

THESIS

Presented to the Faculty of the Graduate School of

The University of Texas at Austin

in Partial Fulfillment

of the Requirements

for the Degree of

Master of Science in Engineering

THE UNIVERSITY OF TEXAS AT AUSTIN

DECEMBER 2014

Acknowledgements

I would first, and foremost, like to acknowledge and thank my advisor Dr. Adela Ben-Yakar of the University of Texas at Austin for her continued support and guidance. Her enthusiasm and passion for multidisciplinary research have inspired numerous beneficial projects and innovations, such as the one described here. Dr. Navid Ghorashian, Dr. Sudip Mondal, and Sertan Kutal Gökçe have been instrumental to the progress of this project and my research education here at UT Austin. I would like to thank Dr. David W. Hahn and Dr. Kamran Mohseni from the University of Florida for providing me with my first research opportunities. Dr. David W. Hahn in specific has provided me guidance beyond the lab, which I greatly appreciate. My fellow lab members have all been instrumental to my educational experience at UT and are all excellent human beings.

AUTOMATED PARALLEL IMMOBILIZATION MICROFLUIDIC PLATFORMS FOR HIGH-THROUGHPUT NEURONAL DEGENERATION STUDIES WITH *C. ELEGANS*

Evan Marley Hegarty, M.S.E.

The University of Texas at Austin, 2013

Supervisor: Adela Ben-Yakar

C. elegans has emerged as an invaluable model organism for in vivo neurobiology research to understand disease mechanisms and pathology relevant in humans. Simple anatomy, short lifecycle, fully characterized genome, and miniature body scale make these nematodes an ideal model organism for phenotyping and bio-molecular studies using microfluidic platforms. Advancements in soft-lithography have improved the functionality of microfluidic technology for *C. elegans*, leading to whole organism studies in high-throughput manner that were not otherwise possible.

In order to study phenomena that require large amounts of data such as drug screens for neurological disorders and phenotyping, high-throughput imaging platforms with high-speed, high-resolution image acquisition become essential. With this in mind, we have developed and tested microfluidic immobilization devices to enable high-throughput optical interrogation of *C. elegans* for neurodegenerative diseases and large scale drug screens. Initially, we designed, developed, and tested single-layer and double-layer SU8 mold PDMS chips with parallel tapered channels to immobilize 40 adult *C. elegans* for high-resolution fluorescence imaging of their neurons in a parallel manner.

We achieved over 90% immobilization efficiency using these initial devices, but could achieve only ~50% of the trapped worms with proper orientation to allow scoring of the VC neurons of interest. To improve worm orientation, we developed a three-layer microfluidic chip that can immobilize and orient the adult worms for optical interrogation of these VC neurons with 90% efficiency. Finally, we scaled the platform to accommodate a large scale platform with standard multi-well format on-chip wells where each well leads to the optimized trapping channels.

The final optimized multi-well platform provides comprehensive easy to use 96-well microfluidic system to orient, immobilize, and image adult *C. elegans* in high-throughput manner. The novel gasket system can pressurize the multi-well device pre-loaded with 96 individual worm populations. Using a sequence of on-off applied gasket pressure, we can orient and immobilize worms in all 96 devices simultaneously in less than 5 minutes. Custom designed software can capture 12 z-stack images per worm from all 96-well in less than 12 minutes. With 95% trapping efficiency, approximately 90% of the worms can be scored successfully for neuronal phenotyping of VC neurons. This 96-well platform and the automated imaging system enable high-throughput optical interrogation of adult *C. elegans* for large-scale drug screens relating to ageing and various neurodegenerative diseases.

Table of Contents

List of Figures

CHAPTER ONE: INTRODUCTION

Neurodegenerative diseases pose an enormous financial and emotional burden on the world. In 2010, 35.6 million people were estimated to have dementia, resulting in a worldwide economic burden of $604 billion US dollars annually [1,2]. Not only are these estimates conservative based on the financial earnings from serious mental illness, but they do not take into account the suffering and huge emotional encumbrance on the patients, families, and caregivers. While the general life expectancy of the world continues to rise, the occurrence of age-related neurodegenerative diseases will continue to escalate. Therefore, identifying potential drug targets rapidly as well as understanding the fundamental basis of neurodegenerative diseases could significantly accelerate the detection of new treatments and therapies for these ailments. Our research group has been developing optical and microfluidic techniques to enhance the study of neurodegenerative diseases in the nematode, *Caenorhabditis elegans* (*C. elegans*).

Over the past 30 years, *C. elegans* has moved to the forefront of developmental biology and neurobiology research relating to humans [3]. *C. elegans* is an ideal model organism for high-throughput in vivo studies of bio-molecular phenomena due to its short lifecycle, fully sequenced genome, and fully stereotyped neuronal wiring. The numerous experiments enabled by *C. elegans*, combined with the inexpensive cost and ease of cultivating these nematodes in large numbers, have led to them becoming a widely used model organism in research labs, pharmaceutical labs, and environmental agencies around the world. Over the past ten years, three Nobel Prizes (in Physiology, Medicine, and Chemistry) have been awarded to researchers studying *C. elegans*.

Microfluidic technologies have become a ubiquitous tool in chemical and life sciences over the last two decades. Microfluidics have helped to increase the throughput

and precision of experiments with *C. elegans*, enabling important neurobiology investigations [4] and many experiments that are otherwise impossible. The next generation of microfluidic devices for these experiments should be easy to use, simple to connect between the macro and micro world, and allow a much greater throughput to gather large amounts of data, useful for high-throughput drug screens (why is large amount of data important for aging studies?). With this in mind, we have developed, designed, fabricated, and tested microfluidic devices to enable high-throughput optical interrogation of *C. elegans* for neurodegenerative diseases and large scale drug screens. First, we developed a simple single-layer microfluidic device from molded polydimethylsiloxane (PDMS) to immobilize and image Day 3 adult *C. elegans*. The device consists of an array of 40 tapered parallel traps, each to immobilize a single adult *C. elegans* for fluorescent imaging and observation without using anesthetics. A wedge shaped clamping device developed by Hulme et al. [5] could achieve ~90% immobilization with 126 parallel traps but required approximately 15 min to complete the loading process due to its branching geometry. With our single layer device, nearly 50% of are found to be oriented in an unfavorable position for imaging. This study led to our development of a two-layer and subsequently a three-layer SU8 mold PDMS device, the goal of which is to not only rapidly immobilize the adult *C. elegans*, but to simultaneously orient them laterally during the filling of the traps. These goals were successfully achieved using the three-layer SU8 mold PDMS device with specific aspect ratio design for the immobilization channels. Next, we began to develop a multi-well format to connect the devices for high-throughput investigations. We began by designing a two-well PDMS device using a well plate format. Each well, which was built into the chip, led to 40 immobilization channels, separated by 9 mm spacing, and the trapping channels of two wells connected to a single common exit. We further expended the chip

to include 8-wells and 16-wells. In the 16-well platform every 8 wells connected to a single common exit. The wells were pressurized from a single pressure source with a custom built gasket. After theoretically optimizing the flow characteristics and redesigning the exit channels for the 16-well platform, we were able to obtain similar flow rates from each well and successfully orient, immobilize, and image greater than 90% of the loaded worms.

Finally, using the optimized 16-well platform, we developed a comprehensive easy to use 96-well microfluidic system for high-throughput orientation, immobilization, and imaging of adult sized *C. elegans*. To control, align, and house the device, we designed and built a novel gasket system that inserts directly into the microscope stage. Using this system, we can orient and immobilize the worms from all 96 devices simultaneously using a single pressure source. In order to acquire high resolution z-stack images from all the devices rapidly, in a parallel effort, our group developed a custom built LabVIEW algorithm to control the motion of a high speed microscope stage and a large field-of-view camera. Utilizing this algorithm, we were able to attain high resolution z-stack images of all 3,840 animals with our inverted fluorescent microscope in less than 12 minutes. This 96-well platform and system enables high-throughput optical interrogation of adult *C. elegans* for large-scale drug screens relating to aging, Alzheimer's disease, Huntington's disease, and many other neurodegenerative disorders.

CHAPTER TWO: MOTIVATION AND BACKGROUND

C. elegans have emerged as an invaluable model organism for in vivo high-throughput neurological and biological research relating to humans. *C. elegans* are miniature, optically transparent, non-parasitic roundworms that are found in temperate soil environments around the world. They are the first multicellular organism to have its genome completely sequenced and the only organism to have its neuronal wiring diagram (connectome) completed. These traits, combined with the short life cycle and the inexpensive cost and ease of cultivating these nematodes in large numbers, make them an ideal model organism. Furthermore, because the body length scales of *C. elegans* are on the order of microns to around a millimeter, these nematodes are easily and quickly manipulated in microfluidic devices.

Microfluidics technology has emerged as a powerful tool to increase the throughput and precision of experiments with *C. elegans*, enabling many important neural cell biology investigations [4] that are otherwise impossible. Recent advancements in soft-lithography that improve functionality and adaptability of microfluidic technology for *C. elegans* has led to whole organism high throughput and high resolution studies that were not possible otherwise [6]. Various other microfluidic technologies have been demonstrated for *C. elegans* involving sorting [7], long-term culture [8,9], fluorescent based screening [10-12], three-dimensional imaging [13,14], time-lapse imaging with optical manipulation [15], and other integrated microfluidic platforms [16]. These devices range from single channel to more complex designs with multiple layers for high-resolution imaging and phenotyping using fluorescent markers. *C. elegans* provides an in vivo model with a high level of complexity that resembles disease pathology in humans, which is advantageous for understanding disease mechanisms and progression, and for

elucidating disease pathways [17-20]. *C. elegans* have made large contributions to the biological study of ageing using the WormFarm [8] and anti-aging role of polydatin [9]. Real time drug screening in *C. elegans* [21], serially orienting worms to study neuronal processes for developmental defects [9], immobilization of worms using wedged shaped channels [5], laterally orienting worms [10], stress response and study of physiological process of individually confined worms (WormSpa) [22], and liquid culture high throughput screening of *C. elegans* [23-25] have been demonstrated, with many using microfluidic devices. The next generation of microfluidic devices for these experiments should be easy to use, simple to connect between the macro and micro world, and allow a much greater throughput for gathering large amounts of data. With this in mind, we have designed, developed, and tested microfluidic devices to enable high-throughput optical interrogation of *C. elegans* for neurodegenerative diseases and large scale drug screens.

CHAPTER THREE: EXPERIMENTAL ASPECTS

In this chapter we present the specific scientific and technological details relevant to the work presented in this thesis. We will discuss the *C. elegans* stains used as well as their culturing techniques for large numbers for high-throughput studies. Then we will discuss the microscope stage and optical imaging setup used for the study. Next, we will demonstrate the fluid dynamic modeling for our microfluidic devices. Finally, we will discuss the fabrication method for our microfluidic devices and device flow rate characterization methods. These technologies, combined with the speed and facility of using *C. elegans* as a model organism, will enable high-throughput investigations and screens that can lead to discovery of new drug compounds and significant progress in understanding the mechanism of neurodegenerative diseases.

3.1 *C. elegans* strains and culturing techniques

We used two *C. elegans* strains for our Alzheimer's disease study. LX959 and JPS67 worms were used as the wild type and APP mutant strain respectively [26]. In both of these strains, the motor neurons VC1-VC6 were marked with green fluorescent proteins (GFP) that can be visualized using fluorescent microscopy. The strains of *C. elegans* were initially grown and maintained on nematode growth medium (NGM) agar plates with HB101 bacteria at 20 °C according to the standard methods [27].

High-throughput drug screens using *C. elegans* require worm culturing and liquid handling in large quantities and in parallel. It is difficult to grow large numbers of *C. elegans* on NGM plates in laboratory environments. The difficulties in growing these large quantities for drug screens range from maintaining a food supply for each drug compound until the worms reach the adult stage, non-uniform drug exposure over time on a two dimensional habitat, altered food concentration with time, and the need for multiple

worm transfers during one single experiment. To overcome these challenges, we adopted liquid culture maintenance of *C. elegans* and modified the protocol to suit our need for drug treatments.

C. elegans strains are maintained and synchronized at 20 °C for large population of liquid culture worms for high throughput studies in devices. Four healthy larval stage 4 (L4) hermaphrodite are transferred to a 10 cm diameter NGM plate containing HB101 bacterial lawn at 20 °C. The plate produces ~900-1000 gravid worms in 7 days which is then bleached to obtain ~6000 viable eggs on bleaching. The bleached eggs are incubated at 20 °C in a 360 degree rotor for 24 hours for all the eggs to hatch and obtain age synchronized larval stage 1 (L1). Hatched L1s are cleaned by filtering through a 20 μm filter that separated healthy L1s from unhatched eggs, unhealthy/dead L1s, and worm carcasses present in the liquid. Healthy L1s are collected in a glass tube and centrifuged at 1000 rpm for 2 min to achieve a worm density of ~100 worms/10 μL of liquid. A volume of 20 μL is dispensed in 32 wells of 24-well plates with an additional 1 mL of HB101 bacterial food in S. medium ($1x10^9$ cells/mL). The worms are incubated at 20 °C and shook at 80 rotations per min (rpm) for 48 hours until they reach late L4 stage. The well plate is left on a horizontal surface for 10 min for the worms to sink down to the bottom of the well. 1 mL of freshly suspended HB101 is added in every well. 50 mL of FUDR (8.4 mM in water) is added to every well to avoid production of new young worms in the well volumes. Appropriate drug compounds are added in designated wells at known concentrations. The plates are incubated for 72 hours until the worms grow to day 3 adult (D3) stage. Each well of the 32 wells are dispensed to three wells on a 96 well plates with a 40 μm filter sieve. Worms are filtered, rinsed, and transferred to a fresh 96-well collection plate. Finally, the worms are pipetted from individual wells to the wells of a primed device to be used for imaging using high-throughput screening platform.

3.2 Optical imaging setup and stage

All bright field and fluorescent images are acquired using an Olympus IX73 inverted microscope equipped with a 4 megapixel large field of view CCD camera (Princeton Instruments). Images are acquired using 2x (0.06 NA) and 10x (0.3 NA) objectives for bright field and fluorescence imaging, respectively. The fluorescent imaging system consists of a mercury lamp and a GFP filter set. The excitation filter and the emission filter transmit wavelength ranges of 460-500 nm and 510-560 nm respectively. We utilize an in-house LabVIEW program to move a motorized stage with a flat-top XY translational stage and a high resolution piezo stage for Z movement. The custom LabVIEW program controls the stage and camera to acquire and save z-stack fluorescent images for all 40 immobilization channels in each chip for the whole 96-well device. A full 96-well device generates 4608 fluorescent z-stack images (~40 GB of images) in less than 12 minutes.

3.3 Fluid dynamic modeling of flows in microfluidic chips

The design and development of microfluidic chips require prior device experiences and modifying devices in conjunction with analytical and empirical mathematical modeling using fluid mechanics to meet our experimental need. The basic conceptual chip design and its layout is guided by experience from prior published work by our group [28] and other microfluidic researchers [5], while mathematical models allow us to optimize fluid flow profiles and flow rates.

In order to calculate the necessary fluid flow characteristics for a microfluidic system, one can reduce the system to a fluidic circuit using the Hagen-Poiseuille law, discussed later in this section [29]. **Figure 3.3.1** displays a basic fluidic circuit model of a

microfluidic system with flow driven by a constant pressure source. The fluidic resistances of all the major components are calculated based on their geometries as well as the pressure drop across each component. The inlet to the system can be given a designated pressure and the outlet gauge pressure is assumed to be zero (atmospheric pressure). Once the fluidic pressure entering the chip is determined, the expected flow rates and velocities within a given microfluidic system can be calculated using analytical mathematical models.

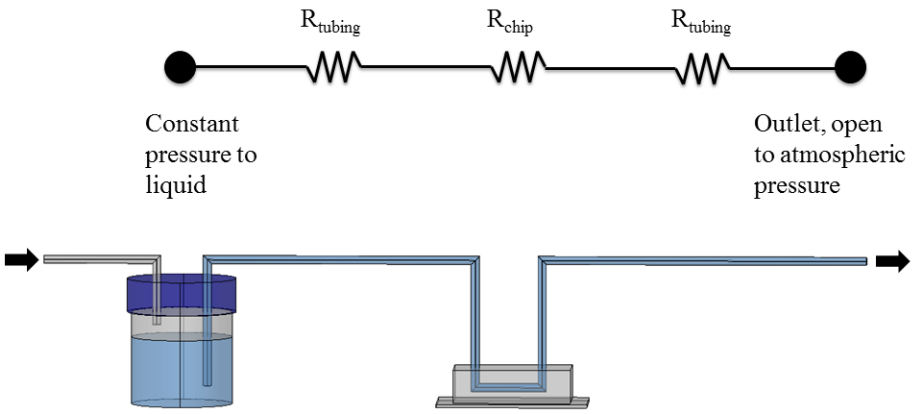

Figure 3.3.1: Fluidic circuit model.
Schematic of a basic fluidic circuit model of a microfluidic system with flow driven by a constant pressure source. A fluid source under a constant known gauge pressure is fed to the chip from tubing and then exits the chip through additional tubing to atmospheric pressure. R_{tubing} is the fluidic resistance of the tubing either before or after the chip. R_{chip} is the total fluidic resistance of the microfluidic device.

An important fluid mechanics parameter to consider in the design of microfluidic devices is the Reynolds number. The value of the Reynolds number is a ratio of the inertial forces to the viscous forces and is determined by Eq. (1).

$$Re = \frac{\rho Q d}{\mu A} \quad (1)$$

Here, ρ is the density of the fluid, d is the diameter of the given tube, Q is the volumetric flow rate of the fluid, μ is the viscosity of the fluid, and A is the cross-sectional area of the tube. High Reynolds numbers (>2000) generally indicate that turbulent mixing will occur within the fluid. Low Reynolds numbers generally indicate laminar flow, or streamline flow, which is when fluid in a channel or tube travels in parallel layers with no mixing between layers. Low Reynolds numbers are often expected at microfluidic length scales and fluid velocities, so laminar flow profiles tend to dominate [30].

Fluidic resistances for the tubing connections, which externally interface into the microfluidic chip, are estimated from the characteristic equations describing fully developed laminar flow of a Newtonian fluid in a circular tube, as shown in Eq. (2)

$$R = \frac{128 \mu L}{\pi d^4} \quad (2)$$

Here, μ is the fluid viscosity, L is the length of the tube, and d is the diameter of the tube. Since the resistance has a $1/d^4$ dependence on the tube diameter, small changes of the diameter can lead to significant changes in fluidic resistances.

For our microfluidic device, the fluidic resistance across the micro-channels is determined using an alternative method, since the channels have rectangular cross-sections with dimension on the order of tens of microns. In order to get an analytical solution for the fluid resistance of micro-channels, we solve the Navier-Stokes equations for an incompressible, isothermal, isotropic liquid flow with no slip boundary conditions

at the rectangular walls. The final expression to estimate microfluidic resistance in a rectangular cross-section, as described in [30], is shown below.

$$R = \frac{12\mu L}{wh^3}\left[1 - \frac{h}{w}\left(\frac{192}{\pi^5}\sum_{n=1,3,5}^{\infty}\tanh\left(\frac{n\pi w}{2h}\right)\right)\right]^{-1} \quad (3)$$

Here, h is the height and w is the width of the rectangular channel. L is the length of the channel section for which we are calculating the resistance and μ is the viscosity of the fluid. We will continue to utilize Eq. (3) for our resistance calculations. For the devices and tubes used in our experiments and discussed in this thesis, the resistance of the tubing leading to the devices are calculated to be less than 0.1 % of the resistance of the entire chip due to the large difference in the cross-sectional dimensions within the channels of the device versus the tubing diameters.

With the fluidic resistances calculated based on device geometries and the known pressure drop across the entire system, we calculate the flow rate of the system using the Hagen-Poiseuille Law [29]. The parameters are related to each other by the simple fluidic circuit model shown in Eq. (4),

$$\Delta P = QR \quad (4)$$

where ΔP is the pressure drop, Q is the volumetric flow rate, and R is the fluidic resistance across the particular channel. Using this relation, we can then calculate the pressure drop and flow rate through each resistance element throughout the entire chip design.

3.4 Microfluidic device fabrication

Our microfluidic devices are fabricated using three-layer photo-lithography and soft-lithography techniques. We first designed the photo masks using AutoCAD 2013 and had them printed on transparencies using 40K DPI resolution laser-plotter (Fineline Imaging). In brief, a 6 inch silicon wafer is first spin coated with SU8-2025 photoresist (Microchem Corp.) at 2100 revolutions per minute (rpm) for 33 seconds to obtain a uniform height of ~45 μm (Layer-1, red). The layer is exposed to UV light using a photo-mask with the pattern for layer-1 (mask-1), as displayed in **Figure 3.4.1** (A). This layer is hard baked and developed to remove the unexposed SU8 photoresist. A second layer of SU8-2025 is spin coated at 1900 rpm for 33 seconds to obtain a height of ~65 μm (Layer-2, green). The second layer is exposed to UV light using a photo-mask with the pattern for layer-2 (mask-2), as shown in **Figure 3.4.1** (B). This layer is then hard baked and developed to remove the unexposed SU8 photoresist from layer-2. A third layer of SU8-2035 photoresist (Microchem Corp.) is spin coated at 1650 rpm for 33 seconds to obtain a height of ~85 μm (Layer-3, blue). The third layer is then exposed to UV light with a photo-mask with the pattern for layer-3 (mask-3), as displayed in **Figure 3.4.1** (C). The third layer is hard baked and developed to remove the unexposed SU8 photoresist from layer-3. The SU8 mold with all three layers is treated with tridecafluoro-1,1,2,2-tetrahydrooctyl-1-trichlorosilane vapor (United Chemical Technologies) in a vacuum chamber at -67 KPa and 40 °C to create a hydrophobic layer to reduce surface adhesion during the soft-lithography process.

Polydimethylsiloxane (PDMS, Dow Corning) is mixed at a ratio of 10:1 (base to curing agent) and poured on the silanized SU8 mold with a 96-well PCR plate positioned on top of the SU8 features such that every well is aligned and placed on top of the circular pad at the entrance of every parallel immobilization device. The PCR plate is also pre-coated with silane vapor in a vacuum chamber to ease its release after the PDMS has cured. An acrylic outer mold (acr) is placed on the silicon substrate with SU8 features to restrict outer dimensions of the PDMS mold and achieve a device height of around 8 mm of PDMS, as shown in **Figure 3.4.1** (D). The PDMS layer is cured at 70 °C for 2 hours, peeled off from the SU8 mold, and released from the PCR plate. The PDMS block is punched for the 12 designated exits and for the bottom of all 96 wells using a manual punching machine (Accu-Punch MP10-UNV, Syneo). The PDMS block is then cleaned and bonded to a 1/8 inch borosilicate glass substrate via oxygen plasma treatment of 110 Watts. The bonded device is cured at 70 °C for 6 hours to enhance the glass to PDMS bonding, shown in **Figure 3.4.1** (E).

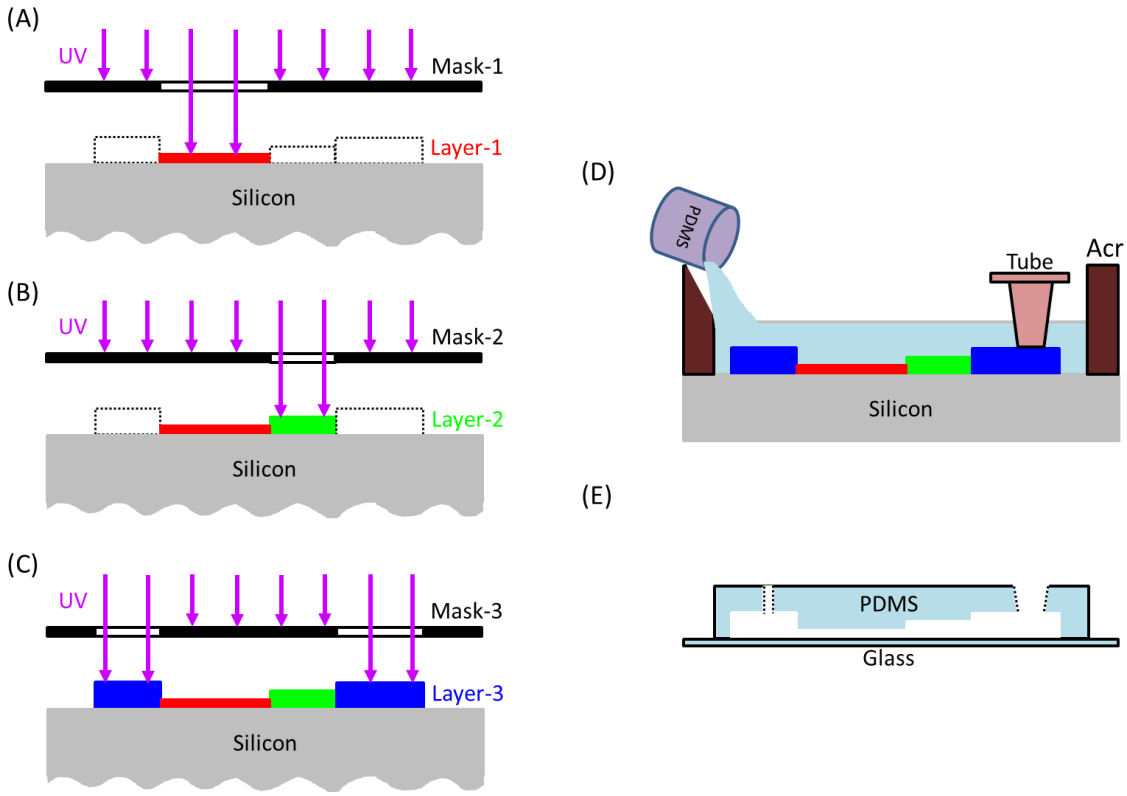

Figure 3.4.1: Three-layer microfluidic device fabrication.
Schematic of device fabrication. Multi-layer photo-lithography is used to fabricate Layer-1 (A), Layer-2(B), and Layer-3 (C) out of SU8 photo-resists on a silicon wafer using high resolution plotted masks, mask-1, mask-2, and mask-3 respectively. The three layers are exposed and developed for three different heights (~45 µm, ~65 µm, and ~85 µm respectively) to obtain desired aspect ratios on the silicon wafer. (D) PDMS 10:1 mixture is poured on the SU8 layered silicon mold using an acrylic support (Acr) and a silane vapor treated 96-well PCR conical tubes for well structures on top of the well pads at the entrance to each device. (E) PDMS mold is cured at 70 °C for 2 hours, peeled off from the silicon substrate, removed from the 96-well PCR plate, punched with holes for external connections, and bonded to a 1/8 inch glass substrate.

3.5 Flow rate characterization

For flow rate measurements, PDMS devices are fabricated from the three-layer mold with input punches to be able to insert a metal coupler for flow input. A pressure buffer line at 10 psi is connected to one of the devices while all other inlets are blocked

using metal plugs. The device is primed to remove any air bubbles using the pressurized inlet with a blocked exit line for 30 minutes. Flow rates are measured by collecting buffer through the exit for 20 seconds at every pressure value (2.5, 5.0, 7.5, and 10.0 psi). This output volume is collected at least three times for every device and pressure value. Exit number 3 connecting well number A05-D06 of a 96-well device with the gasket system is opened to collect the volume of buffer from all 8 wells connected with the same exit.

CHAPTER FOUR: PARALLEL IMMOBILIZATION MICROFLUIDIC DEVICES FOR HIGH-THROUGHPUT NEURONAL DEGENERATION STUDIES IN *C. ELEGANS*

In this chapter, we describe the design considerations that led to the optimized parallel immobilization microfluidic devices for optical interrogation and neurodegenerative studies in *C. elegans*. We discuss 1), the initial work using single layer tapered immobilization traps and our first design, 2) the subsequent double-layer mold design and our associated challenges, and 3) the triple-layer mold devices and the design considerations that led to the optimized trapping region. We discuss the design and testing of connecting many chips together in a multi-well format in order to greatly increase the speed and throughput of device. We then discuss the novel gasket system used to deliver liquid pressure to each population in a 96-well device from one pressure source. Finally, we describe the total device assembly and flow of the experimental procedure.

4.1 Overview of design considerations

Microfluidic devices have enabled many neurological and biological investigations using *C. elegans* as a model that would have been otherwise impossible. Our goal is to develop the next generation of microfluidic devices that are easy to use, simple to connect between the micro and macro world, and allow a much greater throughput to gather large amounts of data. Whiteside's group has initially demonstrated a microfabricated array of wedge shaped clamps used to immobilize and image live *C. elegans* [5]. While this device is able to successfully immobilize and acquire low

magnification bright field images of trapped worms, its branching network of channels takes a long time to load and immobilize worms. The orientation of the worms is uncontrolled, which can be unfavorable for imaging. Our research group has previously demonstrated a parallel microfluidic device for nerve regeneration studies of L4 stage *C. elegans* [28]. This PDMS device has no branching network connecting to the immobilization channels and allows for much faster loading. Our initial device for optical interrogation of day 3 adult *C. elegans* utilized this same design with increased dimensions to allow the much larger and older worms to be properly immobilized. We found one inherent problem associated with all of these devices; more than half of the immobilized worms are not oriented in a lateral posture suitable for obtaining high quality images of the desired VC neurons. This led to our development of a double-layer device, the goal of which is to not only rapidly immobilize the adult *C. elegans*, but to simultaneously control the orientation of the nematode during the filling of the traps. Our double-layer device can rapidly load and immobilize adult *C. elegans* for fluorescent imaging without anesthetics, but only half of the worms are oriented correctly for imaging. Finally, we designed a three-layer device with suitable aspect ratios for the trapping channels that successfully and rapidly loads, orients, and immobilizes the day 3 adult *C. elegans* in a favorable orientation for fluorescent imaging.

Each of our triple-layer microfluidic chips contains 40 parallel trapping channels. In order to create a device that is high throughput and easy to load, we designed and tested connecting many chips together in a multi-well format. Few research groups have developed well plate based devices for cell studies where a well plate with machined

access holes is bonded on top of a thin polymer microfluidic device such that each well connects to a single liquid input site to each chip [31, 32]. Loading liquid samples containing cells, *C. elegans*, or chemicals into a well using a pipette is much easier and faster than plugging a syringe to a tube with a metal coupler into every small hole leading to a microfluidic device. We decided to design our multi-well devices based on the common 96-well plate format whose design is already utilized by many robotic devices and liquid handling systems. Instead of machining and utilizing a solid plastic well plate bonded to our chips, we use a section (or the entirety) of a 96-well plate as an upper mold when fabricating our PDMS devices. Each well is built into the PDMS device and connects to the entrance of a single chip. We began by designing and testing a 1x2-well device with two chips connected symmetrically to a common exit. Then we developed a 4x2-well device where eight chips, connected in a series of four pairs, connect to a single common exit. After optimizing the output flow rates for different chip locations, we developed and tested a final 96-well device that consisted of 12 eight-well devices leading to 12 exits on the boundaries of the device.

While microfluidic technologies have enabled fast and automated control of biological and chemical samples with great precision, wide-spread adoption of microfluidics in relevant research areas has been hindered by the lack of a simplified interface between the macro and micro world. Our 96-well device helps to mitigate this hindrance by allowing easy sample handling and loading into each of the 96 microfluidic chips. In order to achieve a superior yet simple interface to control the device, we have designed and developed a novel gasket system. This gasket system allows for fluid

control and immobilization of the worms in all 96 chips using a single pressure source. The device is operated using filtered M9 from a 500 mL reservoir pressurized by compressed air. The pressure is transmitted to the top gasket through a computer controlled solenoid valve.

The device assembly and loading methods for our investigation have been optimized to achieve the most simple and robust high-throughput experimental procedure. We have divided the flow of this procedure into three steps: liquid culture worm maintenance, device/worm preparation and immobilization, and image acquisition with data analysis. Utilizing our device assembly, we are able to load and immobilize worms in all 3840 channels in less than 5 minutes with greater than 90% of the loaded worms oriented correctly. Using our automated stage movement and image acquisition algorithm, we can collect all 4608 (~40 GB) z-stack images of the entire device in less than 12 minutes.

4.2 Microfluidic designs and testing

In the following section, we describe the microfluidic designs starting with the simplest device and progressing to the final design used for our high-throughput platform. We present and describe our single-layer device, our three different double-layer devices, and our final triple-layer device with optimized aspect ratio for trapping channels.

4.2.1 SINGLE-LAYER PARALLEL IMMOBILIZATION MICROFLUIDIC DEVICES

Our first design is a simple one-layer microfluidic PDMS chip fabricated using a one-layer SU8 mold on a silicon wafer. The device consists of an array of 40 tapered parallel traps, each to immobilize a single adult *C. elegans* for fluorescent imaging and observation without the use of anesthetics. **Figure 4.2.1.1** (A) displays a 0.7x magnification stereoscope image of the one-layer chip. The chip has one main entrance that fans out to the opening of the 40 parallel traps. There is a single exit connected to atmospheric pressure and a purge line to remove untrapped worms from the device. **Figure 4.2.1.1** (B) displays a schematic representing the channel entrance and exit dimensions as well as the channel height throughout the device. As worms are pressed into the trapping region from a pressure source such as a syringe or pressurized fluid reservoir, the tapering of the width along the channel's length allows for the immobilization of day 3 adult *C. elegans*. **Figure 4.2.1.1** (C) displays an image of the single-layer chip containing 40 immobilized worms in parallel ready for subsequent imaging. **Figure 4.2.1.1** (D) displays a magnified microscope image of a worm from this device immobilized in the trapping region.

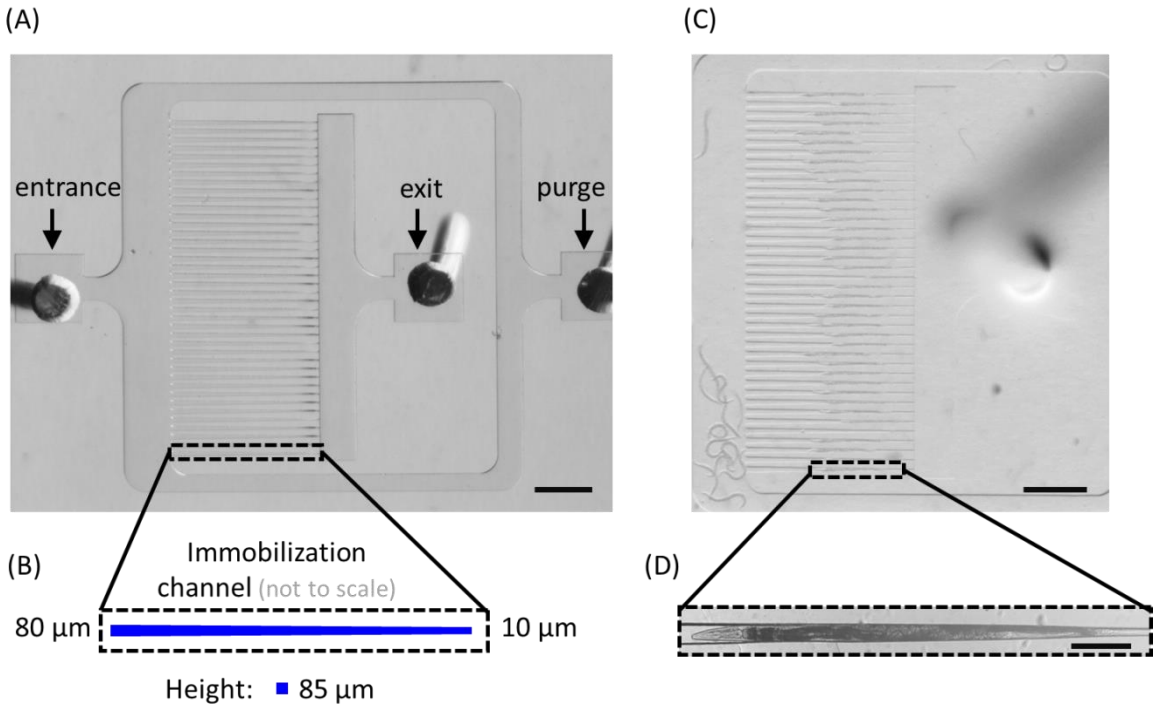

Figure 4.2.1.1: Single-layer parallel immobilization microfluidic device.
(A) A stereoscope image of a single-layer microfluidic device with one entrance, exit, and purge line leading to 40 parallel tapered immobilization channels. (B) Schematic showing the entrance and exit dimensions of the channel as well as the channel height. (C) A stereoscope image of immobilized day 3 adult JPS67 *C. elegans* in a single-layer device. (D) A microscope image of an immobilized adult *C. elegans*. The scale bar is 1 mm (A), (C), and 200 µm (D).

This single-layer PDMS chip showed promising results. 90% of the worms put into these devices are successfully immobilized in the tapered channels. This is achieved within 2 minutes using constant pressure from a syringe (by hand or by pump). While this design has successfully demonstrated rapid loading and immobilization of day 3 adult *C. elegans*, it does not fulfill an important criterion: the successful imaging of motor VC neurons that are the focus of our study. Greater than half of the immobilized worms are

oriented in an unfavorable position for fluorescent imaging of desired neurons. This led to our development of double-layer parallel immobilization chips.

4.2.2 DOUBLE-LAYER PARALLEL IMMOBILIZATION MICROFLUIDIC DEVICES

The goal of the double-layer mold PDMS chips is to not only rapidly immobilize the adult *C. elegans*, but improve the lateral orientation of the nematode during the filling of the traps. All of the subsequent double-layer devices consist of an array of 40 tapered parallel traps, each to immobilize a single adult *C. elegans* for fluorescent imaging and observation. Our double-layer device #1 is a simple one-layer PDMS chip fabricated from a two-layer SU8 mold on a silicon wafer. **Figure 4.2.2.1** (A) displays a stereoscope image of two-layer device #1. This chip has one main inlet and has a height change at the entrance of the 40 parallel traps. There is a single exit connected to atmospheric pressure and a purge line to remove untrapped worms from the device. **Figure 4.2.2.1** (B) shows a schematic of the immobilization channel entrance and exit dimensions as well as the channel heights, depicted in different colors, zone 1 (Z1, blue) and zone 2 (Z2, green). An enlarged image of the two-layer tapered immobilization channels as well as the location of the height change in the device is displayed in **Figure 4.2.2.1** (C).

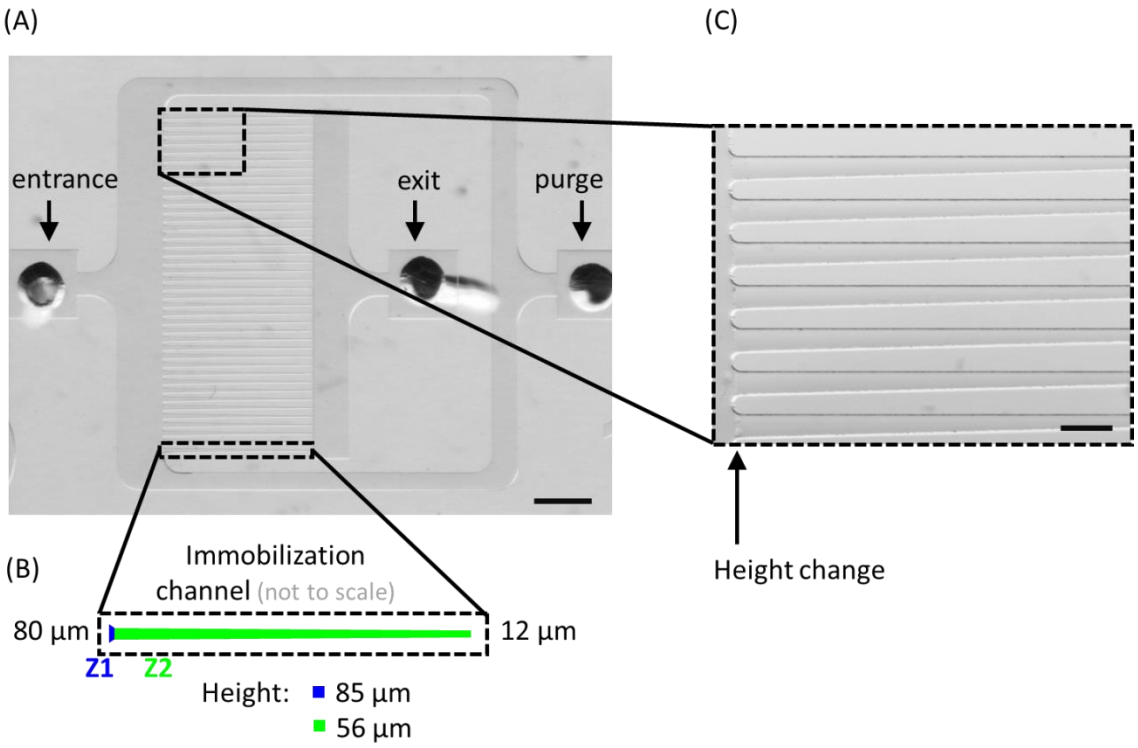

Figure 4.2.2.1: Double-layer parallel immobilization microfluidic device #1.
(A) A stereoscope image of a double layer mold microfluidic device with one entrance, exit, and purge line leading to 40 parallel tapered immobilization channels. (B) Schematic showing the entrance and exit dimensions of the tapered immobilization channel as well as the channel heights, depicted in different colors, zone 1 (Z1, blue) and zone 2 (Z2, green). (C) An enlarged stereoscope image of the tapered immobilization channels. The height change in this device occurs at the entrance of the tapered channels. The scale bar is 1 mm (A) and 200 µm (C).

Our double-layer device #2 is a simple one-layer PDMS chip fabricated using a two-layer SU8 mold on a silicon wafer. A stereoscope image of double-layer device #2 is displayed in **Figure 4.2.2.2** (A). This chip has one main inlet and has a height change that occurs 600 µm from the entrance of the tapered immobilization channels. There is a single exit connected to atmospheric pressure and a purge line to remove untrapped worms from the device.

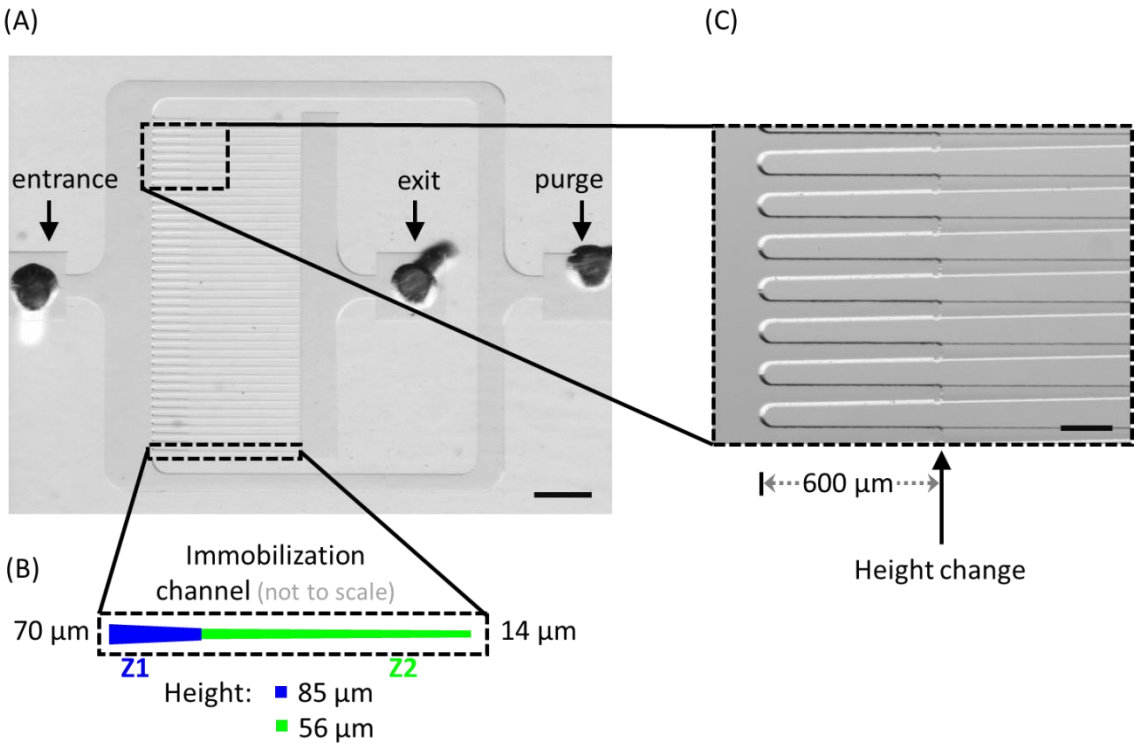

Figure 4.2.2.2: Double-layer parallel immobilization microfluidic device #2.
(A) A stereoscope image of a two-layer mold microfluidic device with one entrance, exit, and purge line leading to 40 parallel tapered immobilization channels. (B) Schematic showing the entrance and exit dimensions of the tapered immobilization channel as well as the channel heights, depicted in different colors, zone 1 (Z1, blue) and zone 2 (Z2, green). (C) An enlarged stereoscope image of the tapered immobilization channels. The height change in this device occurs 600 µm from the entrance of the tapered channels. The scale bar is 1 mm (A) and 200 µm (C).

Figure 4.2.2.2 (B) presents a schematic of the immobilization channel entrance and exit dimensions as well as the channel heights, depicted in different colors, zone 1 (Z1, blue) and zone 2 (Z2, green). **Figure 4.2.2.2** (C) displays an enlarged image of the two-layer tapered immobilization channels as well as the location of the height change in this device. The scale bar is 1 mm in **Figure 4.2.2.2** (A) and 200 µm in **Figure 4.2.2.2** (C).

Our double-layer device #3 is another simple one-layer PDMS chip fabricated using a two-layer SU8 mold on a silicon wafer. **Figure 4.2.2.3** (A) displays a stereoscope image of double-layer device #3.

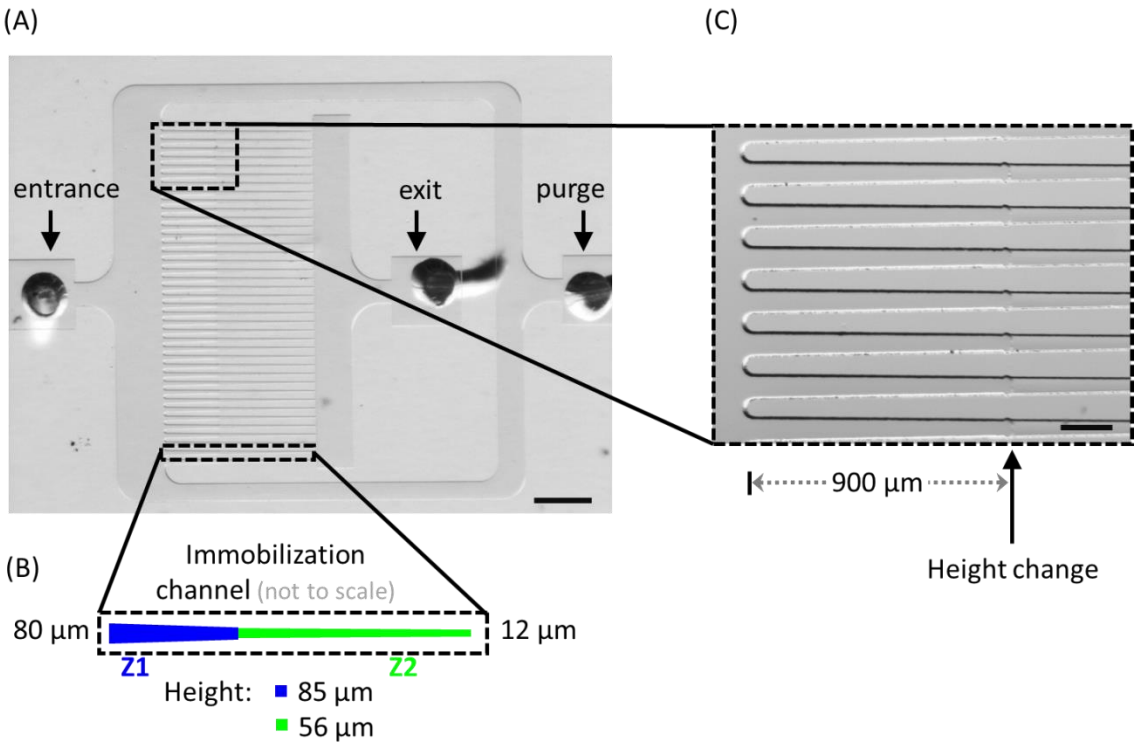

Figure 4.2.2.3: Double-layer parallel immobilization microfluidic device #3.
(A) A stereoscope image of a two-layer mold microfluidic device with one entrance, exit, and purge line leading to 40 parallel tapered immobilization channels. (B) Schematic showing the entrance and exit dimensions of the tapered immobilization channel as well as the channel heights, depicted in different colors, zone 1 (Z1, blue) and zone 2 (Z2, green). (C) An enlarged stereoscope image of the tapered immobilization channels. The height change in this device occurs 900 µm from the entrance of the tapered channels. The scale bar is 1 mm (A) and 200 µm (C).

This chip has one main inlet and has a height change that occurs 900 µm from the entrance of the tapered immobilization channels. There is a single exit connected to atmospheric pressure and a purge line to remove untrapped worms from the device.

Figure 4.2.2.3 (B) shows a schematic of the immobilization channel entrance and exit dimensions as well as the channel heights, depicted in different colors, zone 1 (Z1, blue) and zone 2 (Z2, green). **Figure 4.2.2.3** (C) displays an enlarged image of the two-layer tapered immobilization channels as well as the location of the height change in this device.

These two-layer mold PDMS chips also achieved fast loading and immobilization in the tapered channels for 95% of the worms put into these devices. This was achieved within 3-5 minutes using constant pressure from a syringe (by hand or by pump) or with suction using a vacuum line. While this design also has successfully demonstrated rapid loading and immobilization of day 3 adult *C. elegans*, it still does not achieve the successful imaging of VC neurons that are the focus of our study. 45-50% of the immobilized worms are oriented in an unfavorable position for fluorescent imaging of the desired neurons in this two-layer device. This led to our development of three-layer parallel immobilization chips with more controlled and variable aspect ratios.

4.2.3 TRIPLE-LAYER PARALLEL IMMOBILIZATION MICROFLUIDIC DEVICES

The goal of the triple-layer parallel immobilization device is to immobilize the adult *C. elegans* rapidly and to control the orientation of the nematode during the filling of the traps. This triple-layer device consists of an array of 40 tapered parallel traps per well with variable aspect ratio along the channel length to immobilize and orient adult *C. elegans* for fluorescent imaging and observation. Our triple-layer device is a simple one-layer PDMS chip fabricated using a three-layer SU8 mold on a silicon wafer. **Figure**

4.2.3.1 (A) displays a stereoscope image of a three-layer SU8 mold microfluidic device with one entrance leading to 40 parallel tapered immobilization channels and one exit. The three-layer device is rotated 90 degrees from the two- and one-layer devices to facilitate operation and imaging. **Figure 4.2.3.1** (B) shows an enlarged stereoscope image of the tapered immobilization channels. The first height change in this device occurs 600 μm from the entrance of the tapered channels. The second height change in this device occurs 1200 μm from the entrance of the tapered channels. **Figure 4.2.3.1** (C) shows a schematic of the three-layer 40 channel device with three different device sections depicted in different colors, zone 1 (Z1, blue), zone 2 (Z2, green) and zone 3 (Z3, red). The colors represent different channel heights in the device. Also shown is a schematic giving the entrance and exit dimensions of the channel as well as the channel heights. A plot showing the aspect ratio (width to height) along the length of the three-layer immobilization channels is given in **Figure 4.2.3.1** (D). The aspect ratio is calculated using the width of the tapering channel compared to the three constant channel heights.

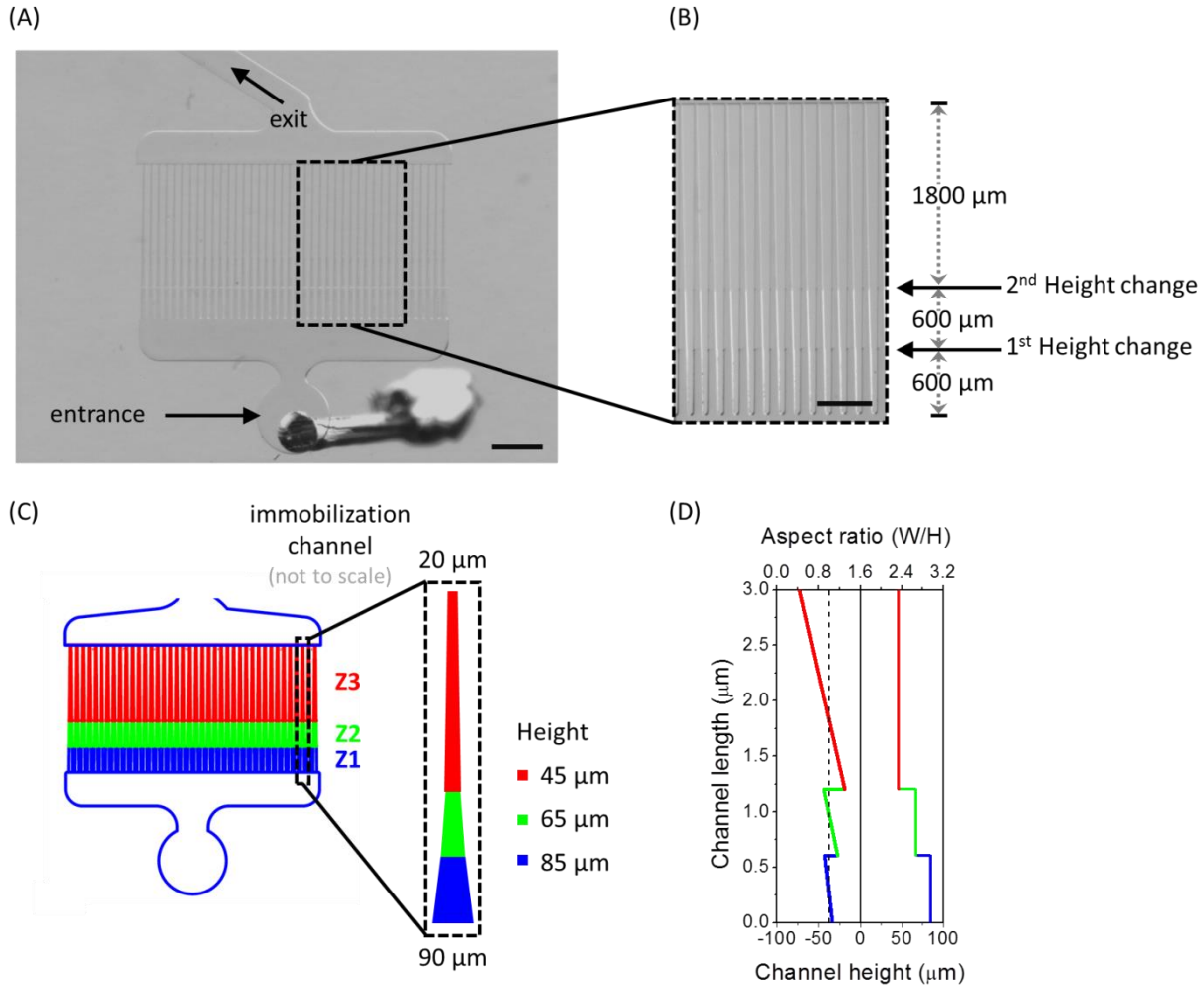

Figure 4.2.3.1: Triple-layer parallel immobilization microfluidic device.
(A) A stereoscope image of a three-layer SU8 mold microfluidic device with one entrance leading to 40 parallel tapered immobilization channels and one exit. (B) An enlarged stereoscope image of the tapered immobilization channels. The first and second height change in this device occurs 600 and 1200 µm respectively from the entrance of the tapered channels. (C) Schematic of the three-layer 40 channel device with three different device sections depicted in different colors, zone 1 (Z1, blue), zone 2 (Z2, green) and zone 3 (Z3, red). The colors represent different channel heights in the device. The inset shows an enlarged schematic giving the entrance and exit dimensions of the channel as well as the channel heights. (D) A plot showing the aspect ratio (width to height) along the length of the three-layer immobilization channels. The scale bar is 1 mm (A) and 500 µm (B).

This three-layer mold PDMS chip achieves fast loading and immobilization in the tapered channels with 95% trapping efficiency. This is achieved within 3-5 minutes using constant pressure from a syringe (by hand or by pump) or from a custom gasket system, discussed later in Chapter 4. Worm entrance and exit channels are fabricated with largest thickness (85 μm, shown in blue **Figure 4.2.3.1** (C)) to reduce physical stress on worms inside the device during the loading process. Worms are found with reduced motion as they are pushed inside the device to the 65 μm (green) and 45 μm (red) sections with multiple immobilization pressure cycles. The width of the channel is varied along the length to achieve aspect ratio values within 1.2-0.4. Day 3 adult worms are immobilized in the region with ~1.0 aspect ratio. These channels are designed with a cross sectional areas of 7650 μm^2 at the entrance and 900 μm^2 at the end of the 3 mm long design. The tapering shape of the channel allows a 3 day adult *C. elegans* with an average body diameter of 75 μm to swim freely at the entrance, but get trapped as it moves along the length of the channel. This design not only successfully demonstrates rapid loading and immobilization of day 3 adult *C. elegans*; it also correctly orients the majority of the worms laterally for successful imaging of motor neurons VC1-VC6, which are the focus of this study. Around 90% of the immobilized worms are oriented in a favorable position for fluorescent imaging of the desired neurons in this triple-layer device. The triple-layer trapping channels with variable aspect ratios are designed based on worm size and morphology in order to coax the worm into a desired orientation for imaging of the VC neurons.

4.3 Multi-well format and flow rate characterization

Total assay time in high-throughput studies is an important parameter. By reducing experimental time per run, one can screen a larger number of compounds which increases the possibility of finding new hits in a chemical screen. In order to create a device that is high throughput and easy to load, we designed and tested connecting many chips together in a multi-well format. We designed our multi-well devices based on the standard 96-well plate format which can be integrated with enumerable robotic stations and liquid handling systems. A 96-well plate is used as an upper mold when fabricating our PDMS devices. In this process, we achieve an exact separation of 9 mm between each pair of wells embedded in the bulk PDMS layer. Each well exhibits a conical shape that connects to a single chip at the bottom.

We started with a 1x2-well design by connecting two chips in parallel leading to a common exit. A schematic of the two sets of chips connected in parallel leading to a common exit is displayed in **Figure 4.3.1** (A). The difference between the two devices is an altered entrance region, leading to different loading behaviors. The chip design with uniform rectangular entrance design achieved rapid immobilization with higher percentages of trapped worm in shorter time compared to the design with triangular entrance. After choosing the best entrance design we developed a 4x2 well devices where eight chips, wired in a pair of four identical chips, and connect to a single common exit. **Figure 4.3.1** (B) shows a schematic of the 4x2-well design with four pairs of chips connected in parallel leading to a common exit. The 4x2-well devices are pressurized from a single pressure source with a simple custom built gasket. Flow rates from a given

pressure source depend on the hydraulic resistances which are a function of the geometrical shape of the microfluidic channels. Since the primary contributor to the hydraulic resistance is exit channel length, flow rate decreases with the relative position of the well with respect to the outlet punch. The well situated on first row and closest to the exit presents minimum total hydraulic resistance and maximum flow rates (**Figure 4.3.3** (A)). Flow rate reduces by ~50% for the well which is farthest from the exit. The variation in the flow rates is more prominent at higher well pressures. To reduce the effect of well location on flow rates, hydraulic resistances are required to be modulated by compensating channel lengths with altered channel widths. For this, we designed an optimized 4x2-well device, as shown on the right side of **Figure 4.3.1** (E).

Hydraulic resistances are calculated for every section of an 8-well device with rectangular cross section (length (L), width (w), and width (h)) using Eq. (3).

$$R = \frac{12\mu L}{wh^3}\left[1 - \frac{h}{w}\left(\frac{192}{\pi^5}\sum_{n=1,3,5}^{\infty}\tanh\left(\frac{n\pi w}{2h}\right)\right)\right]^{-1} \quad (3)$$

The channel is assumed to be filled with a solution having viscosity (μ). The 3 mm long tapered immobilization channel is approximated with 600 segments of 5 μm long channels with varying cross sections connected in series. **Figure 4.3.1** (C) and **Figure 4.3.1** (D) present a fluidic circuit representing the hydraulic resistance components for each section of the four sets of chips connected in parallel leading to a common exit. All resistances are connected with input and output pressure values of P and P_0 respectively.

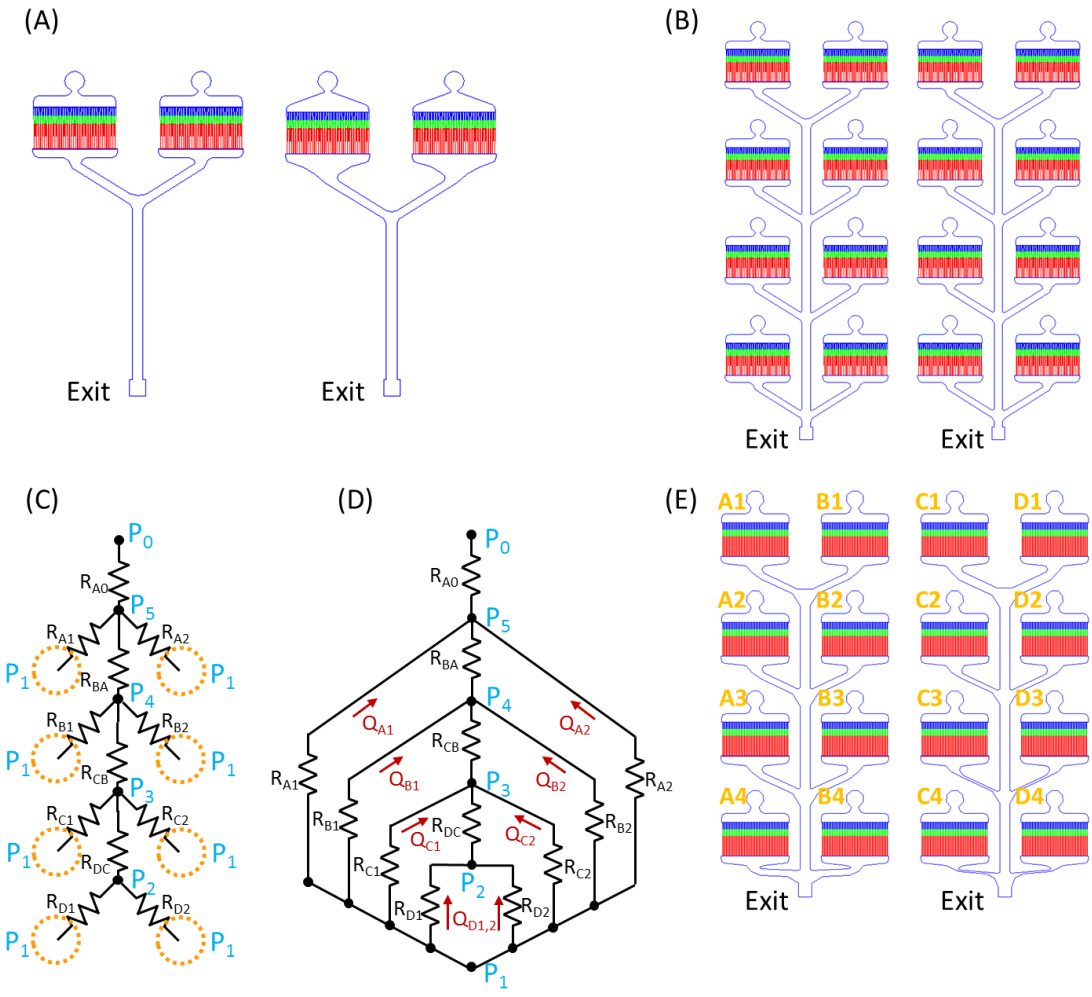

Figure 4.3.1: Development and flow optimization for multi-well three-layer microfluidic immobilization device designs.

(A) Schematic of two sets of 1x2-well chips connected in parallel leading to a common exit. (B) Schematic of two different designs of 4x2-well chips with different entrance designs and connected in parallel to a common final exit. (C) Fluidic circuit representing the hydraulic resistance components for each section of the four sets of chips connected in parallel leading to a common exit and pressurized from one common source. (D) The same fluidic circuit rewritten and used for flow rate optimization. In both (C) and (D) the equivalent resistance of all 40 parallel trapping channels is connected in series with the exit flush arm and represented as R_A, R_B, R_C, and R_D for all 4x2 wells. The exit channel resistances are calculated separately as R_{DC}, R_{CB}, R_{BA}, and R_{A0} between the junctions. All resistances are connected with input and output pressure values of P_1 and P_0 respectively. The hydraulic resistances are iteratively optimized to achieve similar values for flow rates Q_A, Q_B, Q_C, and Q_D using an equivalent circuit. (E) Schematic showing the initial design of the exit arm flush (left) and the optimized exit arm design (right) for the 4x2 devices.

The equivalent resistance of all 40 parallel trapping channels is connected in series with the exit flush arm and represented as R_A, R_B, R_C, and R_D for all 4x2 wells (**Figure 4.3.1** (C) and (D)). The resistances of the exit channels are calculated separately as R_{DC}, R_{CB}, R_{BA}, and R_{A0} between the junctions. The hydraulic resistances are iteratively optimized to achieve similar values for the flow rates Q_A, Q_B, Q_C, and Q_D using the equivalent circuit in **Figure 4.3.1** (D). **Figure 4.3.1** (E) displays a schematic of the initial un-optimized design of the exit arm flush (left) compared to the optimized exit arm design (right) for the 4x2-well devices. Wells A1-B4 in **Figure 4.3.1** (E) have identical channel designs but different net hydraulic resistances for every well up to the final exit. Wells C1-D4 in **Figure 4.3.1** (E) have different channel designs to achieve nearly identical hydraulic resistance up to the final exit, resulting in nearly identical flow rates from each well.

Finally, using the optimized eight-well platform, we developed a comprehensive easy to use 96-well microfluidic system for high-throughput orientation, immobilization, and imaging of adult sized *C. elegans*. **Figure 4.3.2** (A) displays a schematic of the final 96-well device, which is divided into smaller batches of 8-well sections each having a common exit port. Both pairs of 6 exit ports on the two sides of the PDMS block align with a common gasket exit grooves on each side (Exit 1 and Exit 2). **Figure 4.3.2** (B) shows a schematic of the final 8-well optimized design used in the 96-well device. **Figure 4.3.2** (C) shows the final chip design with the optimized exit channel and pillars added to improve structural integrity near the exits of the device.

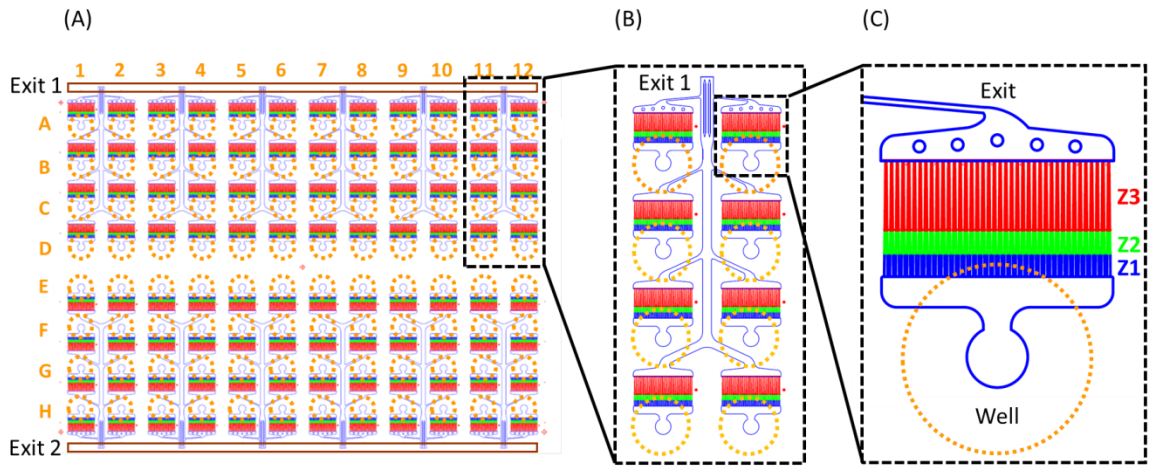

Figure 4.3.2: Final high-throughput 96-well three-layer parallel immobilization microfluidic device.
(A) Schematic of the final 96-well device, which is divided into smaller batches of 8-well sections, each connected together to one common exit port. Both pairs of 6 exit ports on the two sides of the PDMS block align with common gasket exit grooves on two sides (Exit 1 and Exit 2). (B) Schematic of the final 8-well optimized design used in the 96-well device. (C) Schematic of the final chip design with the optimized exit channel. The three different device sections depicted in different colors, zone 1 (Z1, blue), zone 2 (Z2, green) and zone 3 (Z3, red), represent different channel heights in the device.

Flow rates for the initial eight-well device with identical exit channel designs are presented in **Figure 4.3.3** (A). Flow rates are measured using four different well pressures. Higher pressures produce a greater variation in flow rates between the wells. The optimized eight-well design with variable exit channel dimensions, giving nearly equivalent net hydraulic resistances, produces similar flow rates for all the wells, as displayed in **Figure 4.3.3** (B). The optimized design is scaled up for the 96-well device, which shows similar trends for the flow rates from a section of wells located at the middle (A07-D07) and the edge (A01-D01) of a 96-well device, as shown in **Figure 4.3.3** (C). In an attempt to test the performance of the gasket system for all 96-well

immobilization chips, we measured the flow rates from one single exit connecting all 8 wells under different opening condition. The flow rates measured from a single exit dropped by ~ 2% and 5% when all six and all 12 exit ports are open under 5 psi of gasket pressure as compared to when only a single exit is open, as shown in **Figure 4.3.3** (D).

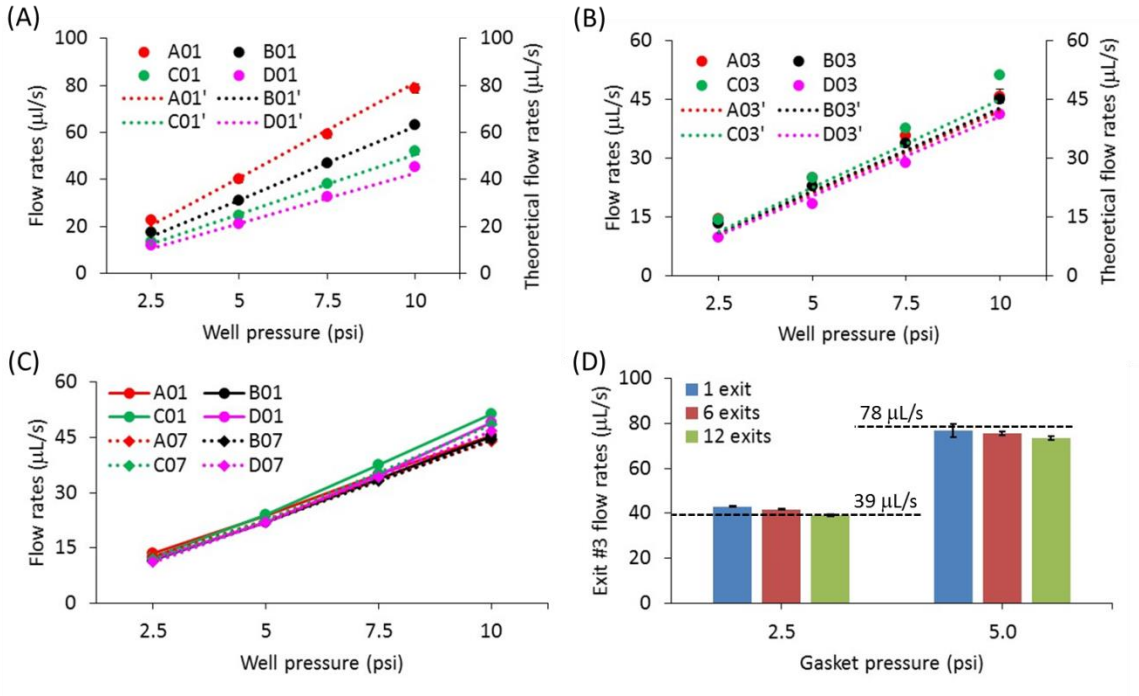

Figure 4.3.3: Flow rate characterization of 8-well and 96-well devices.
(A) Flow rates from a 4X2-well device with identical designs resulting in different flow rates. Flow rates are measured for four different well pressures. (B) Flow rates of a 4X2-well device with different channel dimensions to achieve nearly similar hydraulic resistances. The dotted lines represent the theoretical flow rates as predicted from the resistance optimization. (C) Flow rates from wells at an extreme corner (A01, B01, C01 and D01) and in the center (A07, B07, C07 and D07) of a 96-well device. (D) Exit port #3 flow rates with only the single exit port open, 6 exit ports open, and all 12 exit ports open under the same gasket pressure. Data represented as mean ± SD (n=4).

4.4 Gasket system

To control, align, and house the 96-well microfluidic device, we designed and built a novel gasket microscope stage insert. This system can orient and immobilize the worms from all 96 devices simultaneously in one simple process using a single pressure source. The gasket system comprises of an acrylic top and an aluminum bottom piece. An acrylic sheet of 1/4 inch thickness is machined for the top gasket with one buffer entry port and one air vent. A volume of 4.4 inches x 3.0 inches x 1/8 inches is milled out at the center of the top gasket to hold sufficient buffer volume on top of the 96 wells embedded in the PDMS block. Two narrow lines are milled from the larger sides of the acrylic rectangle to connect all 6 exit punches on each side of the PDMS block. Both exit channels in the top-gasket are connected to an external waste reservoir using a luer connector fitted with a flexible tube. The size of the bottom gasket is machined to match the flat-top motorized microscope stage insert. Most of the material in the bottom gasket is removed from the middle to reduce material weight and enable fluorescence imaging in an inverted microscope. A small step in the metal gasket matches up with the dimension of the glass substrate of the PDMS device. The top and the bottom gasket pieces are held tight using six screws to avoid buffer leakage during pressurization. The device is operated using filtered M9 from a 500 mL reservoir that is pressurized using compressed air. The pressure is transmitted to the top gasket through a computer controlled solenoid valve. **Figure 4.4.1** (A) gives a 3-dimensional model generated in AutoCAD 2013 showing the bottom and top gasket pieces (Gasket-1 and Gasket-2 respectively), the inlet

and exits of the top gasket, and the 96-well device. **Figure 4.4.1** (B) and (C) display an image of the device and gasket system both opened and closed.

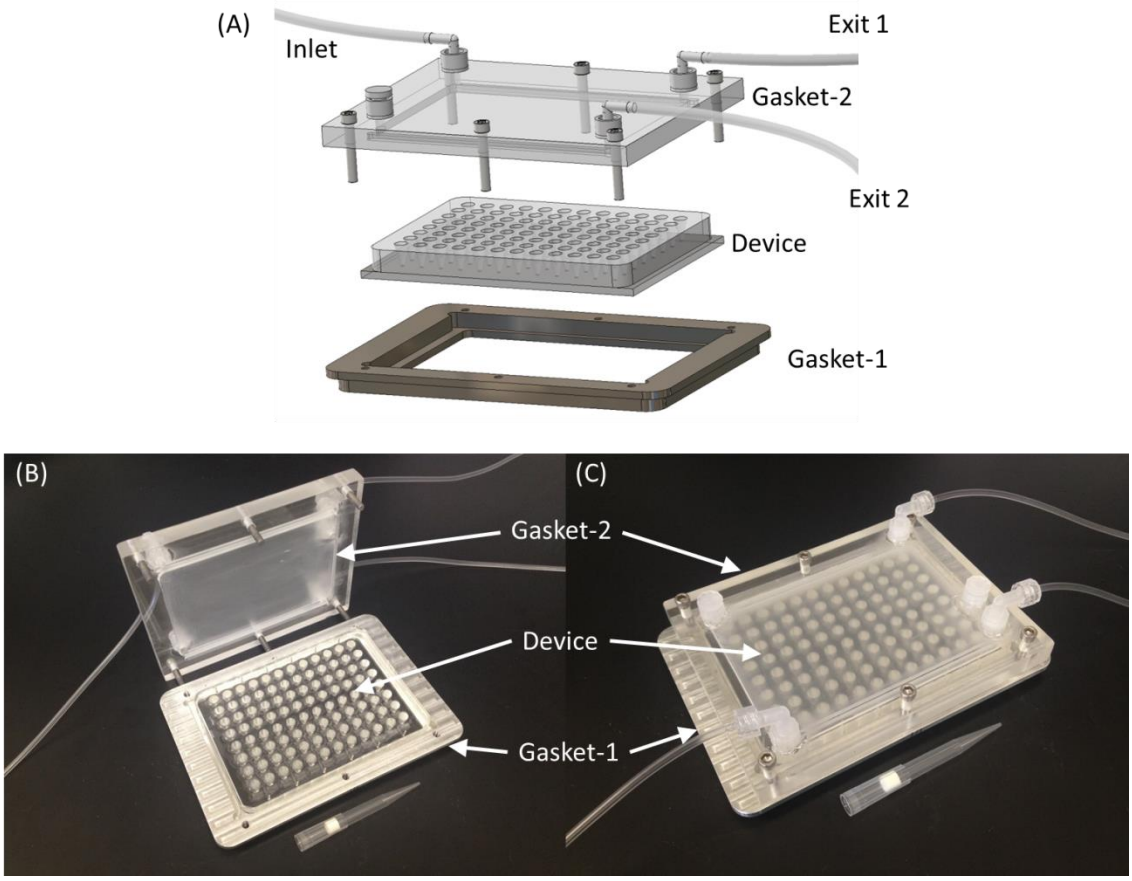

Figure 4.4.1: Gasket system designed for the 96-well microfluidic device.
(A) A 3-dimensional model showing the bottom and top gasket pieces (Gasket-1 and Gasket-2 respectively), the inlet and exits of the top gasket, and the 96-well device. The model was generated using AutoCAD 2013. (B) Image showing the open gasket system containing a 96-well PDMS microfluidic device. (C) Image showing the closed gasket system containing a 96-well PDMS microfluidic device.

4.5 Device assembly and application

Our group has developed a high speed imaging platform for optical interrogation of adult *C. elegans* in a high-throughput manner. **Figure 4.5.1** provides an outline of the

experimental procedure in the form of a flow chart. The chart is separated into three main steps with numerous subroutines. The main steps in order are 1) liquid culture worm maintenance, 2) device/worm preparation and immobilization, and 3) image acquisition and data analysis. The flow chart subroutines give an overview of the preparation, immobilization, optical interrogation, and data analysis of liquid culture grown day 3 adult *C. elegans* in our high-throughput parallel immobilization 96-well microfluidic screening platform.

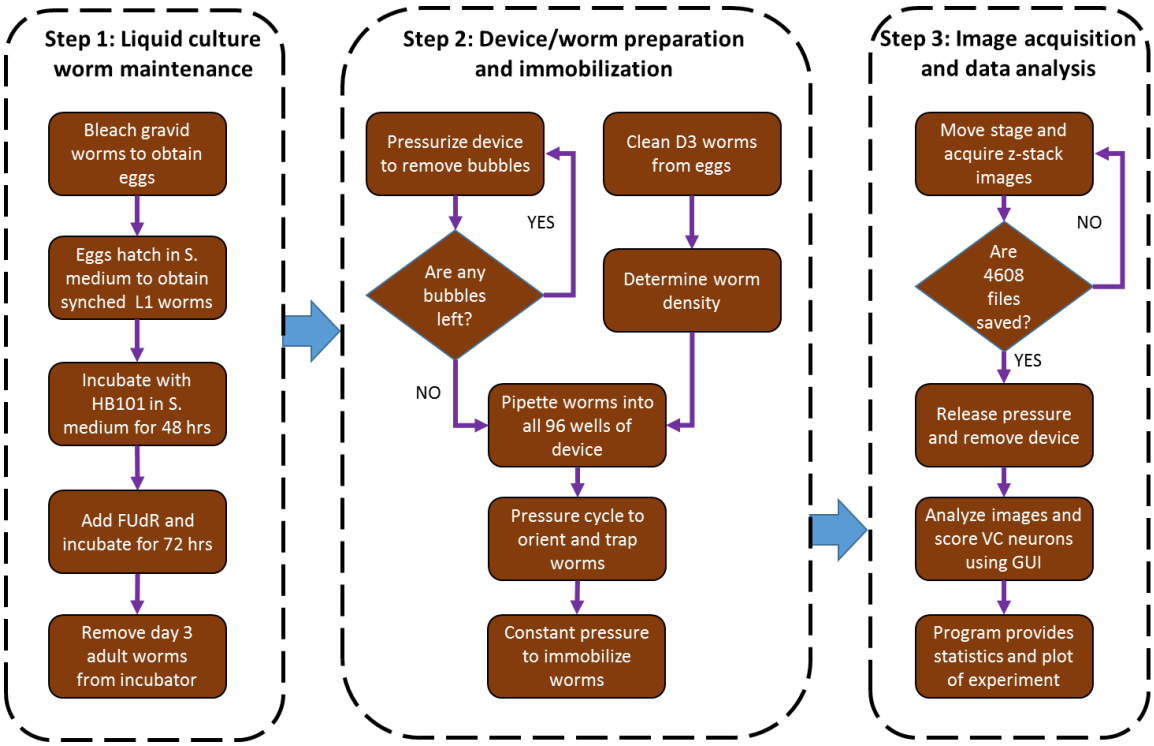

Figure 4.5.1: Experimental procedure flow chart.
A schematic showing the three main steps as well as an overview of the subroutines involved in the preparation, immobilization, optical interrogation, and data analysis of liquid culture grown day 3 adult *C. elegans* in our high-throughput parallel immobilization 96-well microfluidic system.

The screening platform consists of three major hardware components, a 96-well format immobilization device, a motorized stage, and a large field of view camera (**Figure 4.5.2** (A)). The device is designed in PDMS material and is irreversibly bonded onto a 3 mm glass substrate. The PDMS block contains 96 conical shape wells which can hold ~120 μL liquid. Each of the well bottoms is expanded to 40 micro-fabricated channels for worm immobilization. The device is mounted onto an inverted microscope (IX73, Olympus) and held in place using our custom gasket system. The bottom aluminum gasket fits onto the flat-top motorized microscope stage and houses the glass substrate. The top gasket connects to all exits and allows one buffer pressure inlet line. The pressure in the top gasket is controlled using a computer controlled pressure valve. Fluorescence images of the trapped worms are acquired through a 10x, 0.3 NA objective using a 15x15 mm^2 CCD camera. The camera captures 1.5 mm long portion of the ten parallel immobilization channels simultaneously with ~1 μm lateral resolution. A high resolution piezo stage acquires 12 image stacks with 5 μm step size to capture neuronal fluorescence located in different planes. Custom software controls the pressure valve, stage motion, and image acquisition.

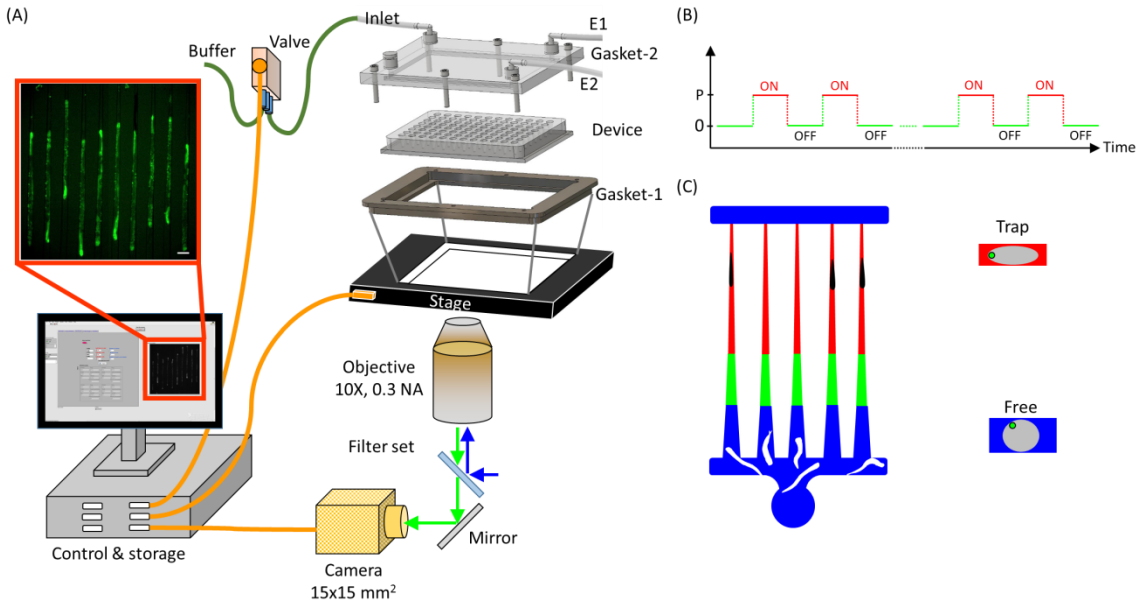

Figure 4.5.2: Schematic of high-throughput platform used for optical interrogation of *C. elegans*.

(A) Shows a schematic of the high-throughput platform developed for *C. elegans* imaging. The platform consists of a multi-well PDMS device clamped in between a gasket system (Gasket-1 and Gasket-2), pressurized by liquid pressure (Buffer), and mounted on a flat-top motorized stage. Fluorescence images of worms immobilized inside the microfluidic device are acquired using a 10x objective (0.3 NA) and a large field of view CCD camera (1.5x1.5 mm^2). The stage, camera, and gasket pressure are controlled and automated using a computer that stores the image files sequentially. Stored images are analyzed and processed using a GUI for phenotyping neuronal health. The red box shows an example of GFP image of 10 worms immobilized inside the parallel traps. (B) Worms are immobilized inside the PDMS device using a computer controlled on-off pressure cycle using a pneumatic valve. Pressure cycles help to orient the worms inside channels. (C) Schematic of a section from the immobilization channel region and the cross-section of a single channel with an adult worm. Worms are relatively free in the first section (blue) and trapped in third section (red) with the ventral side oriented along the channel wall. Scale bar is 100 µm.

The gasket system seals the chip during high pressure cycles for priming and immobilization. Devices are primed for 30 min at 5 psi buffer pressure to fill the whole chip with M9 buffer and to remove any air bubbles in the device. Worms loaded into the well sink to the bottom within 30 s and swim to the channel entrances. Worms in the

whole chip are pushed into the tapered channels using 4 psi gasket pressure. Immobilization pressure is turned 'on' and 'off' for 10 s each for a total of 10 cycles (**Figure 4.5.2** (B)). Worms are pushed inside the channel during 'on' state and released free during the 'off' state to swim and orient themselves. During initial immobilization cycles, worms are freely swimming in channel entrances with 85 μm channel height. As worms are pushed inside the immobilization channel, they become immobile and not capable of changing their orientation. The aspect ratio of the device layers forces the worm to maintain lateral orientation as they are pushed into the channels from the entrances (**Figure 4.5.2** (C)). The device is left with gasket pressure 'on' to keep the immobilized worms in position during imaging. Worms are found to release and escape from the traps with time in the absence of gasket pressure. Alignment features are imaged and measured for device calibration prior to the bright field and fluorescence imaging routine of the whole device. Images are saved in a storage computer and retrieved later for image processing. Images are loaded, processed, and scored to extract useful information such as percentages of healthy worm neurons, degenerated neurons, and worms that are not in good focus. This high-throughput system allows for large drug screens and rapid optical interrogation of 3840 adult *C. elegans* in our 96-well parallel immobilization microfluidic platform.

CHAPTER FIVE: HIGH-THROUGHPUT NEURODEGENERATION STUDIES IN *C. ELEGANS* ALZHEIMER'S DISEASE MODEL

In this chapter, we present an application of our parallel immobilization microfluidic device for high-throughput optical interrogation of adult *C. elegans*. We begin by discussing the neuronal degeneration specific to this investigation. Then we describe the flow and operation of the 96-well device along with the plots and statistics from this study. Finally, we present the VC neuronal degeneration percentages of the control worm and the Alzheimer's disease model worm in our high-throughput platform.

5.1 VC motor neuron degeneration in *C. elegans*

Two strains of *C. elegans* are utilized in this experiment. A wild type worm (WT) with green fluorescent protein (GFP) tagged VC neurons (*LX959*) and an Alzheimer's disease model with a single copy of human APP and GFP tagged VC neurons (*JPS67*). A high-throughput drug screen or optical interrogation of *C. elegans* requires worm culturing and liquid handling in large quantities and in parallel. In order to facilitate these requirements, we have decided to adapt liquid culture maintenance of *C. elegans*, which can be modified to suit our need for drug treatment during a chemical screen. Worms are characterized by their vulva phenotype for drug treatment and/or application of 5-fluoro-2'-deoxyuridine (FUdR), used to prevent eggs from becoming fertile and producing offspring during the study. They are administered for drug treatment at L4 stage and are used for screening and optical interrogation in devices at day 3 adult stage, 72 hours after L4 stage. Worms treated with FUdR at L4 stage in liquid cultures are picked and monitored for neuronal integrity at day1 adult, day 3 adult, and day 5 adult stages of

development. To understand the degeneration patterns, visible GFP signals are imaged on agar pads and scored for neuronal degeneration from wild type (*LX959*) and APP model (*JPS67*) grown in liquid culture and compared with NGM grown animals, as presented in **Figure 5.1.1** (A) and (B). Degeneration percentages from liquid culture worms are similar to the degeneration rates from NGM worms.

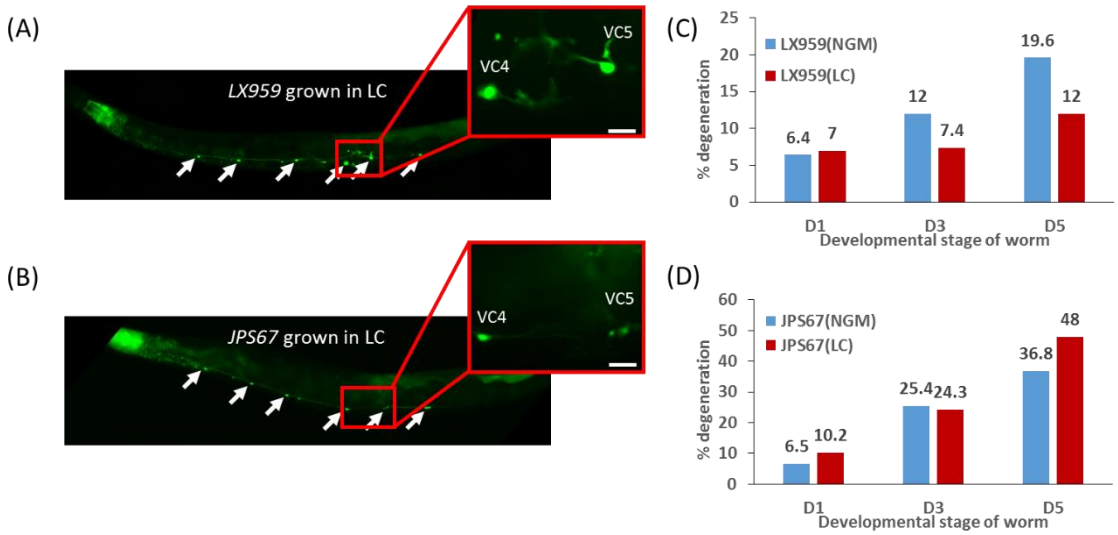

Figure 5.1.1: Alzheimer's Disease model shows higher degeneration with age.
(A) Fluorescence image of day 1 adult WT worm (*LX959*) grown in liquid culture (LC) showing healthy VC neurons. The inset shows high magnification image of VC4 and VC5 neuronal cell bodies of the same worm. (B) Fluorescence image of a day 3 adult APP mutant worm (*JPS67*). The inset shows fluorescence from a degenerating VC5 cell body from the same worm. The white arrows show all six VC neurons. (C and D) Show the comparison of VC4 and VC5 degeneration percentages of *LX959* and *JPS67* animals as a function of their developmental stage. Data represented as mean ± SEM (N>50 animals and N>100 neurons). Scale bar is 10 µm.

Wild type animals growing in liquid culture show 5% degeneration on day 1 stage that increased to 9% and 12% by day 3 and day 5 respectively. This is similar to the percentages found in wild type NGM grown worms (**Figure 5.1.1** (C)). *JPS67* worms show similar degeneration percentages on day 1 (13%), but much greater degeneration

percentages on day 3 (41%) and day 5 (53%), as compared to the wild type control. Similar trend is also observed from the worms growing on NGM plate (**Figure 5.1.1** (D)). Only day 5 stage worms are found to have statistically higher percentages of degeneration in liquid culture compared to the NGM grown worms.

5.2 High-throughput optical interrogation of VC neuron health in adult *C. elegans*

Many *C. elegans* studies, including manual drug screens, are limited to a small number of worms at a time due to various rate limiting factors such as worm immobilization in anesthetic solution, mounting a small number of worms on an agar pad, and manual stage motion to bring individual worms into the field of view for imaging. Using our microfluidic immobilization array, one can immobilize ~4000 worms in parallel to be imaged on top of a flat glass surface and 40 μm high PDMS channels. Worms growing in a 96-well plate are filtered and loaded directly into wells of the PDMS device using a multi-channel pipette. The 96-well device is clamped in between the gasket system before the worms are immobilized inside the channels. The device is mounted on a flat-top motorized XY stage and equipped with a 500 μm piezo for Z movement. All 3-axis motions are controlled using an in-house LabVIEW algorithm, developed in our group. Wells are filled with approximately 60 day 3 adult worms in M9 and clamped with the gasket system to avoid pressure leakage during the immobilization cycle. The top gasket is filled slowly with M9 buffer under 0.5 psi pressure with an air vent open. The slow filling rate avoids worm mixing between wells due to spill over during buffer flow. Worms are able to swim freely at device entrances with the exits closed, but feel the

pressure as soon the exit is opened. Worms are immobilized using an on-off cycle of 4-5 psi on the 96-well gasket system. Exit 1 and exit 2 are opened at same time on both sides to immobilize worms in all 96 wells simultaneously. The whole 96-well immobilization is achieved in less than 5 min and dispenses about 100 mL of buffer volume. One of the wells from D01-E12 is viewed with low magnification (2x, 0.06 NA) to monitor the extent of immobilization with cycle number. Once the immobilization cycle is complete, the stage is manually moved to record XYZ coordinates of wells A01, A12, H12, and H01 using a 10x, 0.3 NA objective to calibrate XY offset and the XZ tilt of the channel design with respect to the stage axes. The XYZ values are calculated for each position on the device and corrected before acquiring the image stacks. The microscope, equipped with a 15 x 15 mm^2 active area and a 10x, 0.3 NA objective, is moved at four successive locations to capture all 40 traps filled with worms per well. **Figure 5.2.1** (A) and (B) demonstrates this lateral movement. At each location, 12 z-stack images are taken at 5 μm intervals to capture neuronal fluorescence located in different planes. A total of 4608 fluorescent z-stack images are acquired from the whole 96-well device in less than 12 minutes. Using this system, greater than 90% of the worms are scored for all 96 wells. Approximately 95% of the immobilization channels per well are filled with worms using our immobilization method, as presented in **Figure 5.2.1** (C). Worms inside the channels do not show any bias for head-tail orientation (55 ± 10%, mean ± SD), as depicted in **Figure 5.2.1** (D). This worm immobilization system provides a uniform platform for high-throughput phenotyping and screening using fluorescent based imaging.

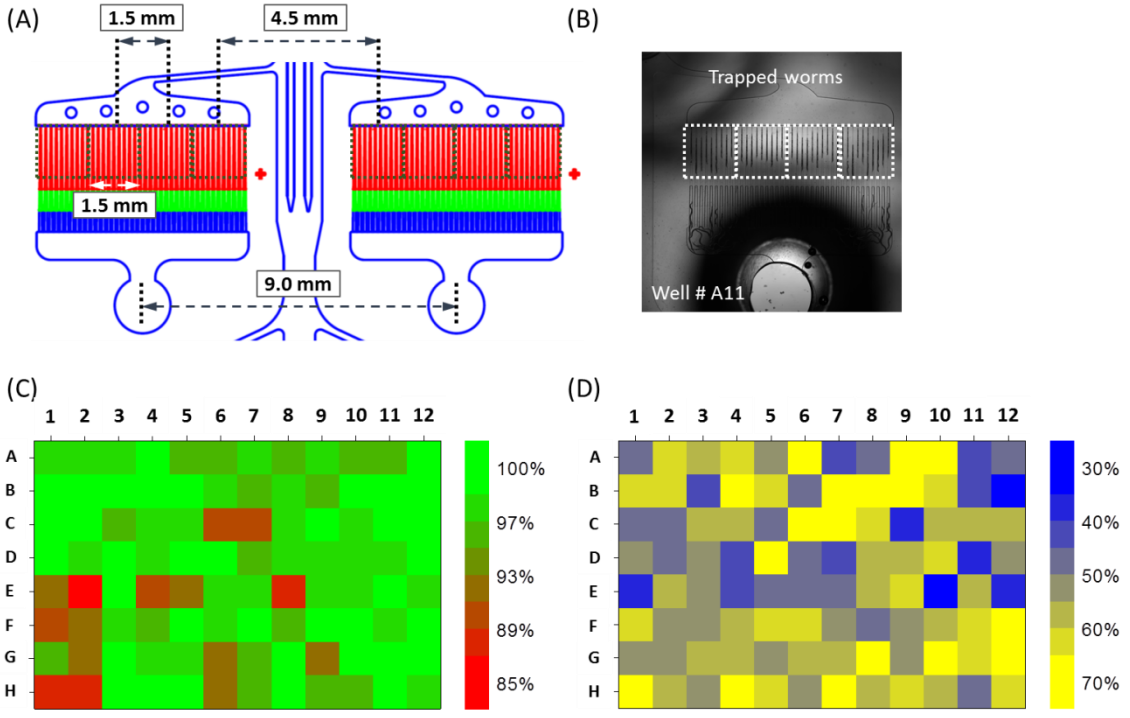

Figure 5.2.1: Stage motion and contour plot of worm immobilization parameters from the 96-well device.

Day 3 old JPS67 worms are immobilized in the 96-well device using 5 psi pressure on the top-gasket. (A) Schematic of the XY stage movement parameters between two consecutive devices. (B) Low resolution image of worms immobilized in the device under well #A11. Parallel traps are imaged with a large camera to capture 1.5 x 1.5 mm and moved in a synchronized manner to acquire 12 z-stack images at every location. (C) Shows the immobilization efficiency map of adult worms from an individual experiment with the 96-well parallel immobilization device. (D) Shows the head-tail orientation of the trapped worms from all 96-well devices with 40 traps per device.

One whole screening of a 96-well device would capture 4608 fluorescent images to be able to phenotype neuronal health from 96 populations in less than 12 minutes. A manual analysis of such a large data set would be a rate limiting factor. Our research group has developed a Graphical User Interface (GUI) based semi-automated image processing algorithm to simplify manual data handling and decrease image analysis time. The GUI has three major parts, locating the worms in the channels, finding the best plane

of focus, and loading cropped images of individual worms for manual scoring. The user can extract the scores to plot them graphically and perform statistical analysis. **Figure 5.2.2** (A) shows a fluorescent image of day 3 adult *JPS67* worms immobilized in our 96-well device during an experiment. Cropped worm images are loaded one at a time for scoring, as displayed in **Figure 5.2.2** (B). The z-stack image with the best plane of focus for VC4 and VC5 of an individual worm is displayed for scoring, as presented in **Figure 5.2.2** (C).

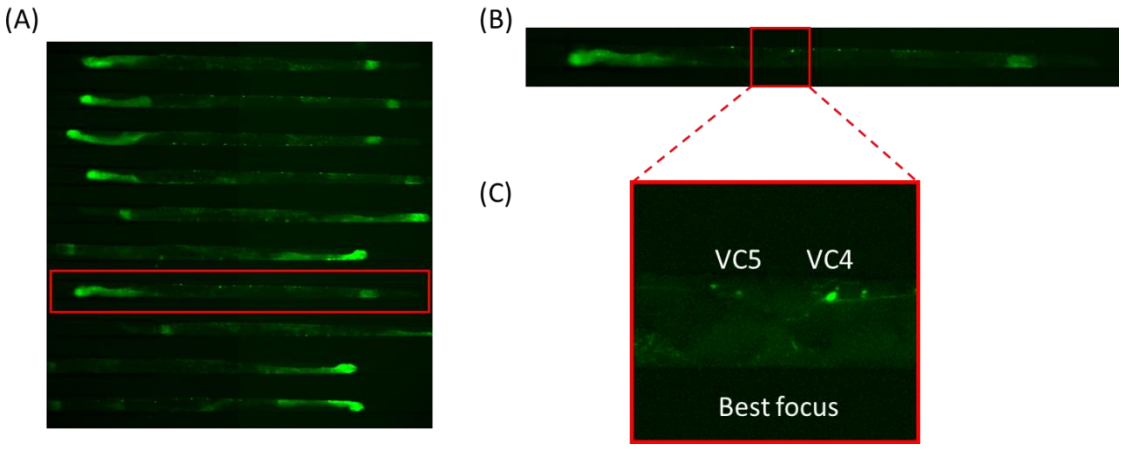

Figure 5.2.2: Scoring of AD model worms (*JPS67*) in the 96-well parallel immobilization device.
(A) Fluorescent image of day 3 adult *JPS67* worms immobilized in the 96-well device. Image taken from a large field of view camera with a 10x 0.3 NA objective using an inverted microscope (Olympus IX73). (B) Cropped fluorescent image of one worm located with the image processing algorithm. (C) Enlarged and cropped fluorescent image of the same worm showing the best plane of focus for VC4 and VC5. The VC4 neuron is healthy while the VC5 neuron is degenerated.

A complete set of images from a full 96-well experiment requires approximately 8 hours to score the ~3840 channels filled with worms for VC neuronal health using our semi-automated GUI. Every single worm is inspected and a score is assigned for VC4

and VC5 in the GUI with an additional remark on the neuronal process. VC4 and VC5 neurons are scored as 'Normal', 'Degenerated', or 'Do Not Score' if they are 'healthy', 'dim/missing', or 'not in focus' respectively. The whole worm is assigned with an additional score for 'Dim Worm', 'Neurons Misshapen', and/or 'Axon Beading' if the whole worm is out of focus, VC4/VC5 cell bodies are misshapen, and/or neuronal process are beaded. The scores for all worms are saved in an array and are assigned with complete identification of the worm. Scores from all 40 traps per well are pulled together to find out degeneration percentages for each population. In one experiment, all 96 wells from one device are loaded with WT worms (*LX959*) and all 96 wells from another device are loaded with APP worms (*JPS67*). **Figure 5.2.3** (A) shows the scored VC neuron degeneration percentages from the whole device with a mixture of *LX959* and *JPS67* worms. Day 3 adult stage *LX959* control worms show a degeneration of 7 ± 4% (mean ± SD) as compared to *JPS67* that shows 24 ± 7% when scored on our high-throughput imaging platform, as displayed in **Figure 5.2.3** (B).

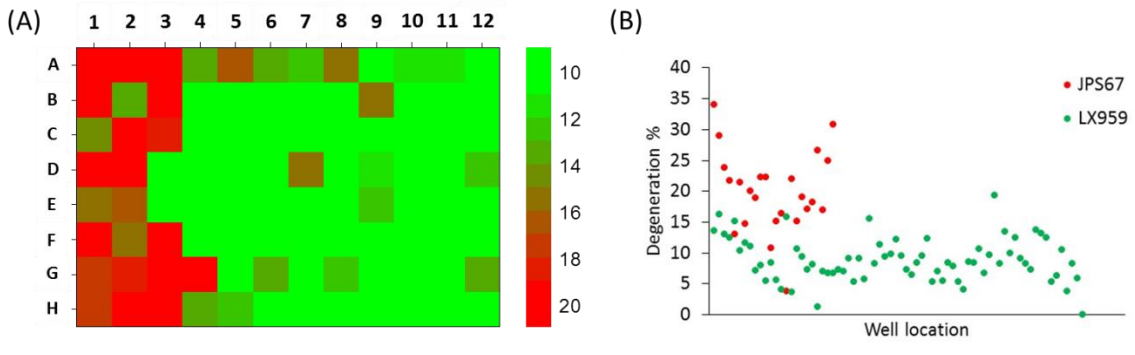

Figure 5.2.3: Semi-automate scoring algorithm with WT (*LX959*) and APP model (*JPS67*) worms on high-throughput platform.

(A) Shows the scores of a 96-well device loaded with D3 stage wild type (*LX959*) worms and APP model (*JPS67*) worms. Degeneration scores from individual wells are represented as shades of green or red. JPS67 worms are loaded into wells A01-H03 and LX959 worms are loaded into the remaining wells. (B) Scatter plot from all 96 wells for both *LX959* (green) and *JPS67* (red).

CHAPTER SIX: CONCLUSIONS AND FUTURE DIRECTIONS

6.1 Conclusions

Numerous microfluidic technologies are available for *C. elegans* research to understand the neurobiology of nerve regeneration [4], stress response of individually confined worms [22], and to facilitate fluorescent based screening [9-11] in vivo. Most of these technologies are laboratory scale since they require complicated valve control, long pre-treatment, serial sample processing, difficult protocols, and are incompatible to existing sample handling. In this thesis, we described the development of a multiple parallel immobilization microfluidic device leading to our triple-layer 96-well microfluidic platform for high-throughput optical interrogation of adult *C. elegans*. Our final 96-well microfluidic based technology has a single pressure input, zero valve control, 30 min pre-conditioning, parallel sample handling, is compatible to multi-well plate handling, and has an easy protocol for non-technologists. The device has twelve segments of 8-well platforms and can be manufactured as a multiple of 8-well configurations. A minimum requirement of one pressure line with maximum 5 psi would allow the user to run the whole chip with an appropriate gasket design. Users are allowed to select any rectangular size well array on the chip to be able to scan predefined well numbers. One complete experiment dispenses ~100 mL of buffer during the whole 96 well experiment. All 96 wells with 40 immobilization channels immobilized approximately 3840 worm in less than 5 min. A shorter immobilization step is very advantageous for sensitive *C. elegans* screens with weaker expression level of fluorescent reporters. Worms immobilized inside the channel can encounter higher level of stress

causing increased auto fluorescence, thus reducing the sensitivity of the screen (poor signal to background ratio).

With an in-house automated imaging platform, we can capture all 40 channels per well in a whole 96-well device in less than 12 min using 10x objective (0.3 NA) and a large field-of-view camera. One full chip scan generates 4608 images of ~ 40 GB data from 3840 worms. The chip is also capable of enabling high resolution imaging screens with higher numerical aperture objectives that would require more z-stacks. A higher NA objective with a smaller field of view would require an increased number of imaging locations to cover the whole length and all 40 channels. Our research group has developed data management through a LabVIEW acquisition system and has developed a separate GUI to analyze fluorescence signals semi-automatically for neuronal phenotypes. Utilizing this GUI, we scored all 3840 channels from a whole 96-well chip in approximately 8 hours. All the scores are pooled together from the multi-dimensional array and displayed for statistical tests.

This screening platform can easily be adapted by a research laboratory for imaging based studies that require large population size phenotyping. Since the device interface is formatted for the standard 96-well platform, the technology can be a great value for commercial infrastructure for large scale high-throughput screening for *C. elegans*.

6.2 Future directions

Our research group is working towards a complete automated image processing algorithm to focus on a specific neurodegenerative disease model where the complete data can be analyzed in less than 30 min. Even though we have used D3 stage *C. elegans* in our screen, one can use the same design principle for different stage of the worm with altered device dimensions to achieve similar efficiency of immobilization. A younger stage worm requires, for example, smaller device dimensions which can allow expansion of the 96-well format to larger well formats.

With this in mind, we have designed, optimized, and fabricated numerous triple-layer microfluidic devices for L4 to young adult stage *C. elegans*. These devices are designed to rapidly orient and immobilize L4 stage worms for semi-automated axotomies using femtosecond laser pulses, optical interrogation of neuronal regeneration post axotomy, and automated high-speed confocal imaging studies in L4 stage *C. elegans*. **Figure 6.2.1** displays the first set of device designs fabricated and tested for these studies. The devices shown in **Figure 6.2.1** (D-F) have multiple exits leading to either individual or double channels to enable long terms studies. Multiple exits allow for precise removal of individual worms or sets of consecutive worms from their trapping channels after each imaging and/or axotomy procedure. These devices are designed to run with L4 stage worms (*zdIs5*) to test the immobilization and orientation of each design. The worms are sent into the devices using a single liquid pressure source of 5 psi gauge. Each design proved to immobilize and orient over 90% of the worms.

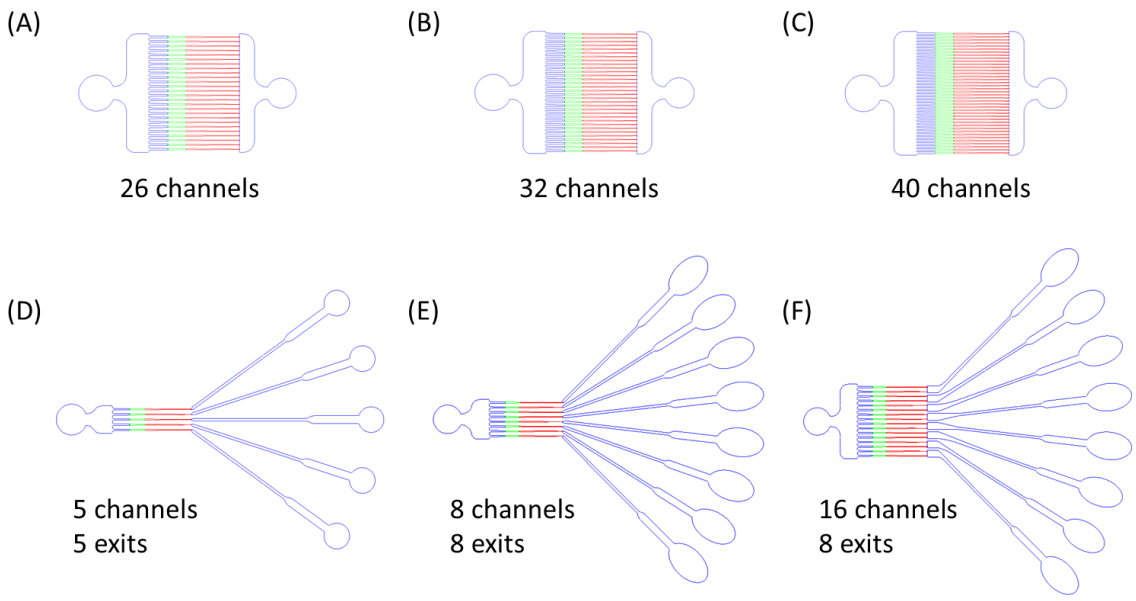

Figure 6.2.1: Triple-layer parallel immobilization microfluidic devices for semi-automated axotomies, neuronal regeneration, and automated high-speed confocal imaging studies in L4 stage *C. elegans*.
The heights and geometries of these devices have been optimized to orient and immobilize L4 to young adult stage *C. elegans* for semi-automated axotomies, optical interrogation, and automated high-speed high-resolution confocal imaging. The three different device sections depicted in blue, green, and red represent heights of 55 µm, 40 µm, and 22 µm respectively. (A) Schematic of a device with 26 channels, each separated by 150 µm. (B) Schematic of a device with 32 channels, each separated by 125 µm. (C) Schematic of a device with 40 channels, each separated by 100 µm. (D-F) The immobilization channels in these devices are separated by 200 µm. (D) Schematic of a device with 5 channels and 5 exits. Each exit can be used to control or remove individual worms. (E) Schematic of a device with 8 channels and 8 exits, which can be used to control or remove individual worms. (F) Schematic of a device with 16 channels and 8 exits. Each of these exits can be used to control or remove two consecutive worms.

In collaboration with Kutal Gokce, the 8-channel and the 26-channel devices are then used to immobilize L4 zdIs5 worms for semi-automated axotomies of the ALM neurons and post-surgery imaging. **Figure 6.2.2** (A) and **Figure 6.2.3** (A) show images of the immobilized worms in the 8-channel and 26-channel devices, respectively. **Figure 6.2.2** (B) and **Figure 6.2.3** (B) show high-resolution images of axons of the ALM neuron cut

using femtosecond laser pulses. **Figure 6.2.2** (C) and **Figure 6.2.3** (C) show images of the same worms immobilized in the device 24 hours post axotomy. **Figure 6.2.2** (D) and **Figure 6.2.3** (D) show high-resolution images of the axonal regrowth 24 hours post-surgery.

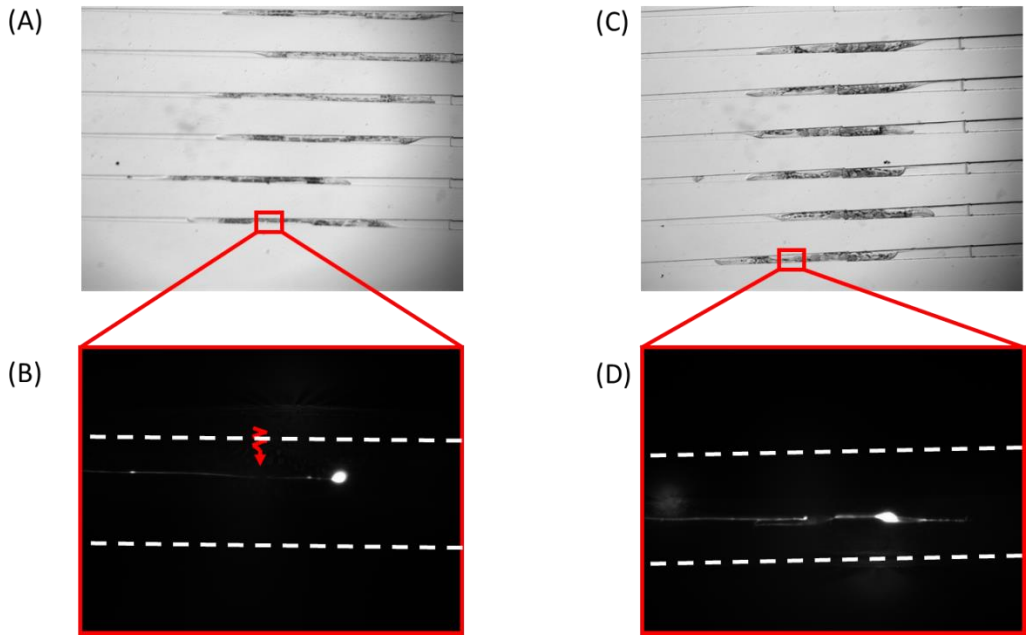

Figure 6.2.2: Semi-automated axotomy experiment using our 8 channel three-layer parallel immobilization microfluidic device with 8 exits.
Successful axotomies were performed on the ALM of 7 out of the 8 immobilized zdIs5 worms, due to proper orientation in the device. (A) Image of immobilized L4 stage zdIs5 worms in our 8 channel device. (B) High-resolution post axotomy image of the ALM cut with a femtosecond laser pulse. The red arrow indicates the location of the cut. (C) Image of the same worms immobilized 24 hours later in our 8 channel device. The device was left with a slow perfusion of S. medium with HB101 bacteria in a 16.5 °C incubator. (D) High-resolution image of regrowth and reattachment of the ALM axon.

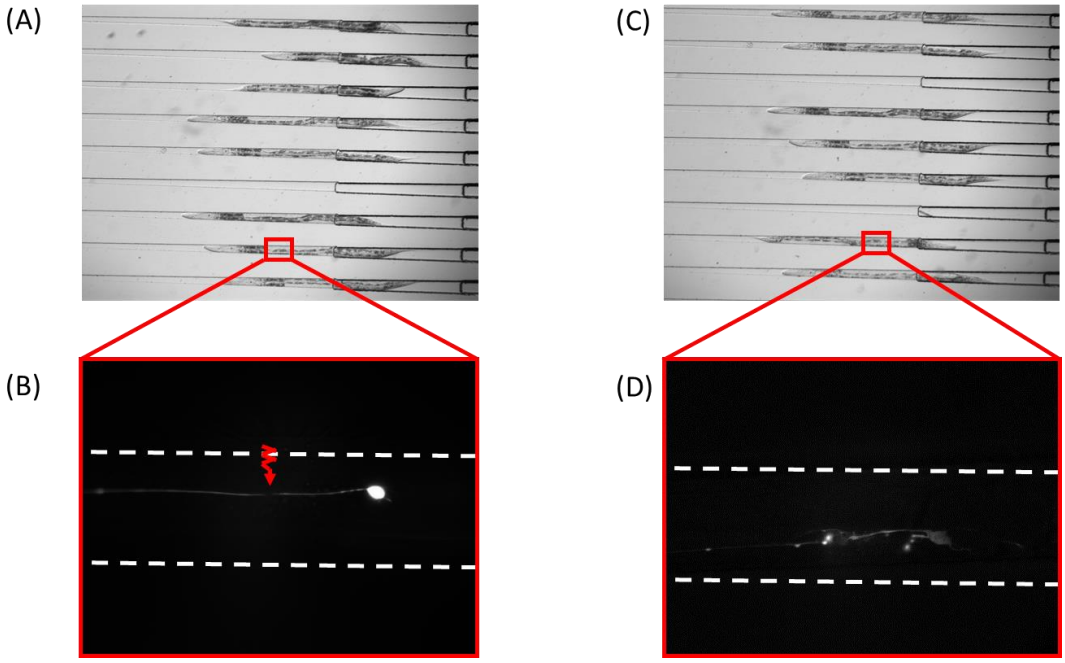

Figure 6.2.3: Semi-automated axotomy experiment using our 26 channel three-layer parallel immobilization microfluidic device.
Successful axotomies were performed on the ALM of 21 out of the 23 immobilized zdIs5 worms. (A) Image of immobilized L4 stage zdIs5 worms in our 26 channel device. (B) High-resolution post axotomy image of the ALM cut with a femtosecond laser pulse. The red arrow indicates the location of the cut. (C) Image of the same worms immobilized 24 hours later in our 26 channel device. The device was left with a slow perfusion of S. medium with HB101 bacteria in a 16.5 °C incubator. (D) High-resolution image of regrowth and reattachment of the ALM axon.

After successful axotomies are performed on over 90% of the immobilized worms, the devices are put into a 16.5 °C incubator with a slow perfusion of HB101 bacteria in S. medium through the device entrance for 24 hours. The worms are then re-trapped in the immobilization channels for post-surgery imaging to understand the level of axon regrowth. This time the worms were immobilized and oriented with around 50% efficiency. This low efficiency is most likely due to the worms getting immobilized in the channels during the 24 hour housing as they are pushed into the trapping channels by the

flow of nutrient perfusion from the device entrance to the channel exits. Worms were found either unhealthy or dead in the channels of the device.

In order to successfully house the worms indefinitely for subsequent imaging and regeneration studies, we have designed a new device with side perfusion channels to allow a slow nutrient perfusion through the housing area of the device. The slow perfusion rates is expected to allow worms to swim freely without getting forced into the immobilization channels during the post-surgery incubation. **Figure 6.2.4** shows the triple-layer parallel immobilization microfluidic device design with perfusion sieve structures. We are currently testing the performance of these devices for nerve regeneration studies that require housing of worms for at least 24 hours.

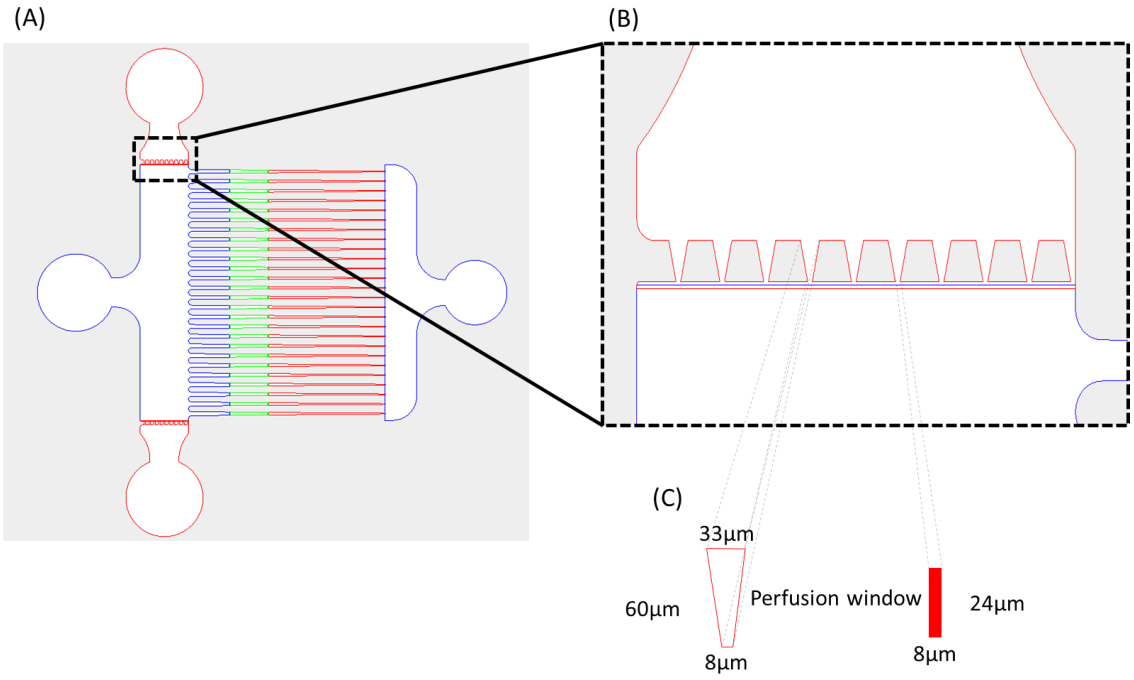

Figure 6.2.4: Triple-layer parallel immobilization microfluidic device with perfusion sieve structures used to house post axotomy L4 stage *C. elegans* indefinitely.

The heights and geometries of this device have been optimized to orient and immobilize L4 to young adult stage *C. elegans* for semi-automated axotomies. The sieve structures allow a slow nutrient perfusion for housing the worms for 24 hours before high-speed high-resolution confocal imaging. The three different device sections depicted in blue, green, and red represent heights of 55 µm, 44 µm, and 24 µm respectively. (A) Schematic of a device with 26 immobilization channels, each separated by 150 µm. The device also has an entrance area that will allow nutrient perfusion for indefinite housing of the worms. (B) An enlarged schematic of the perfusion sieve structures. (C) Schematic of the top and front geometries of the perfusion windows.

Finally, we have designed an initial 384-well parallel immobilization device for ultrafast high-throughput immobilization and imaging of L4 stage *C. elegans*. **Figure 6.2.5** presents the initial 384-well design. Each well leads to parallel immobilization channels designed to orient and immobilize 30 L4 stage worms, for a total of 11,520 worms.

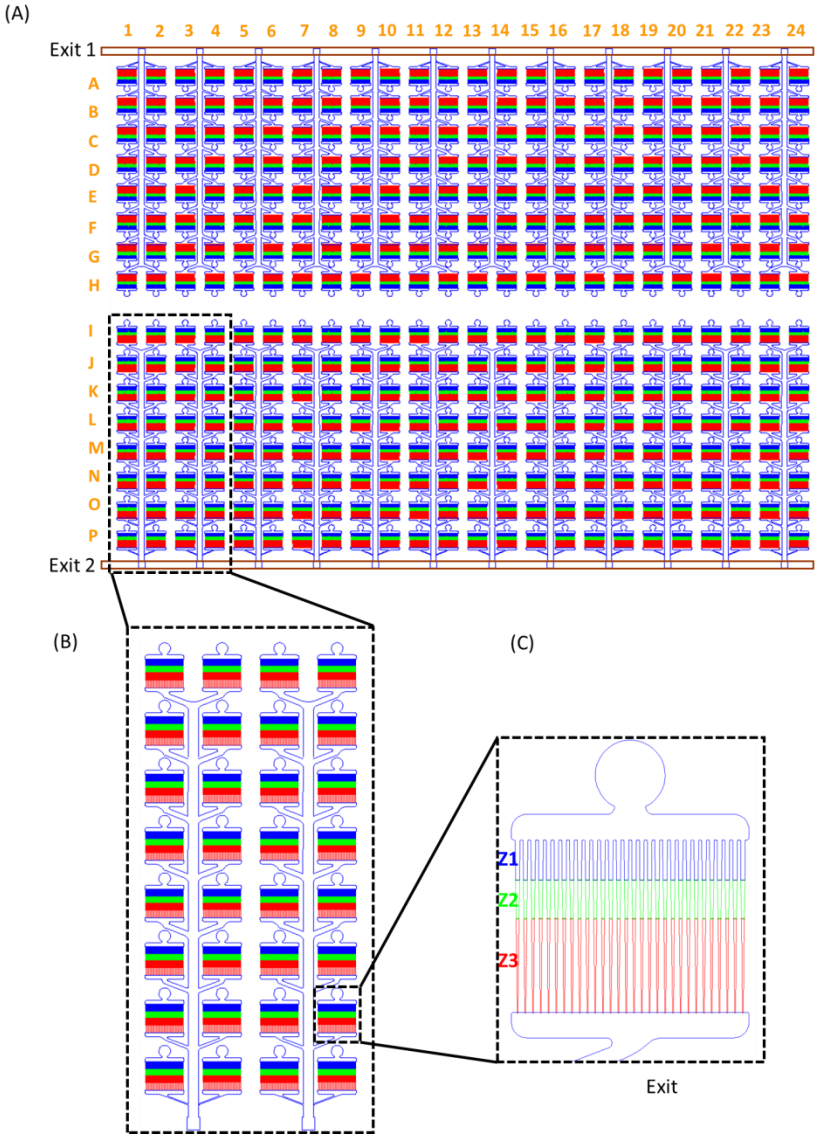

Figure 6.2.5: Ultra high-throughput 384-well three-layer parallel immobilization microfluidic device.

(A) Schematic of a 384-well device design, which is divided into smaller batches of 8-well sections connected together to one common exit port. Both pairs of 25 exit ports on the two sides of the PDMS block align with the common gasket exit grooves on the two sides (Exit 1 and Exit 2). (B) Schematic of the 8-well optimized design used in the 384-well device. (C) Schematic of the final chip design with the optimized exit channel. This design, with 30 immobilization channels per well, has the ability to rapidly immobilize 11,520 worms for optical interrogation. The three different device sections depicted in blue, green, and red represent heights of 55 µm, 40 µm, and 22 µm respectively.

This 384-well platform can be run with the same gasket setup described in the thesis. Since the device interface is formatted for the standard 384-well platform, the technology can be a great value for commercial research labs and large scale high-throughput screening for *C. elegans*. It can be utilized to study Alzheimer's Disease, Huntington's Disease, nerve regeneration in the ALM neuron's axon, and many other neurodegenerative disorders.

References

[1] Kessler RC, Heeringa S, Lakoma MD, Petukhova M, Rupp AE, Schoenbaum M, Wang PS, et al. Individual and societal effects of mental disorders on earnings in the United States: results from the national comorbidity survey replication. Am J Psych, 165: 703–711. (2008)

[2] Insel TR. Assessing the economic costs of serious mental illness. Am J Psych 165: 663–665. (2008)

[3] Gilbert SF. Developmental Biology. 6th edition. Sunderland (MA): Sinauer Associates; 2000. Early Development of the Nematode Caenorhabditis elegans.

[4] Ben-Yakar A, Chronis N, Lu H. Microfluidics for the analysis of behavior, nerve regeneration, and neural cell biology in C. elegans. Curr Opin Neuro, 19: 561–567. (2009)

[5] Hulme SE, Shevkoplyas SS, Apfeld J, Whitesides GM (2007) A microfabricated array of clamps for immobilizing and imaging C. elegans. Lab Chip 7: 1515–1523.

[6] Bakhtina, N. A. & Korvink, J. G. Microfluidic laboratories for C. elegans enhance fundamental studies in biology. Rsc Adv 4, 4691-4709, doi:Doi 10.1039/C3ra43758b (2014).

[7] Ai, X., Zhuo, W., Liang, Q., McGrath, P. T. & Lu, H. A high-throughput device for size based separation of C. elegans developmental stages. Lab on a chip 14, 1746-1752, doi:10.1039/c3lc51334c (2014).

[8] Wen, H., Gao, X. & Qin, J. Probing the anti-aging role of polydatin in Caenorhabditis elegans on a chip. Integrative biology: quantitative biosciences from nano to macro 6, 35-43, doi:10.1039/c3ib40191j (2014).

[9] Xian, B. et al. WormFarm: a quantitative control and measurement device toward automated Caenorhabditis elegans aging analysis. Aging cell 12, 398-409, doi:10.1111/acel.12063 (2013).

[10] Caceres Ide, C., Valmas, N., Hilliard, M. A. & Lu, H. Laterally orienting C. elegans using geometry at microscale for high-throughput visual screens in neurodegeneration and neuronal development studies. PloS one 7, e35037, doi:10.1371/journal.pone.0035037 (2012).

[11] Crane, M. M. et al. Autonomous screening of C. elegans identifies genes implicated in synaptogenesis. Nature methods 9, 977-980, doi:10.1038/nmeth.2141 (2012).

[12] Lee, H., Crane, M. M., Zhang, Y. & Lu, H. Quantitative screening of genes regulating tryptophan hydroxylase transcription in Caenorhabditis elegans using microfluidics and an adaptive algorithm. Integrative biology : quantitative biosciences from nano to macro 5, 372-380, doi:10.1039/c2ib20078c (2013).

[13] Schrodel, T., Prevedel, R., Aumayr, K., Zimmer, M. & Vaziri, A. Brain-wide 3D imaging of neuronal activity in Caenorhabditis elegans with sculpted light. Nature methods 10, 1013-1020, doi:10.1038/nmeth.2637 (2013).

[14] Prevedel, R. et al. Simultaneous whole-animal 3D imaging of neuronal activity using light-field microscopy. Nature methods 11, 727-730, doi:10.1038/nmeth.2964 (2014).

[15] Rohde, C. B. & Yanik, M. F. Subcellular in vivo time-lapse imaging and optical manipulation of Caenorhabditis elegans in standard multiwell plates. Nature communications 2, 271, doi:10.1038/ncomms1266 (2011).

[16] Yang, J., Chen, Z., Ching, P., Shi, Q. & Li, X. An integrated microfluidic platform for evaluating in vivo antimicrobial activity of natural compounds using a whole-animal infection model. Lab on a chip 13, 3373-3382, doi:10.1039/c3lc50264c (2013).

[17] Johnson, J. R., Jenn, R. C., Barclay, J. W., Burgoyne, R. D. & Morgan, A. Caenorhabditis elegans: a useful tool to decipher neurodegenerative pathways. Biochemical Society transactions 38, 559-563, doi:10.1042/BST0380559 (2010).

[18] Dimitriadi, M. & Hart, A. C. Neurodegenerative disorders: insights from the nematode Caenorhabditis elegans. Neurobiology of disease 40, 4-11, doi:10.1016/j.nbd.2010.05.012 (2010).

[19] Calahorro, F. & Ruiz-Rubio, M. Caenorhabditis elegans as an experimental tool for the study of complex neurological diseases: Parkinson's disease, Alzheimer's disease and autism spectrum disorder. Invertebrate neuroscience : IN 11, 73-83, doi:10.1007/s10158-011-0126-1 (2011).

[20] Kaletta, T. & Hengartner, M. O. Finding function in novel targets: C. elegans as a model organism. Nature reviews. Drug discovery 5, 387-398, doi:10.1038/nrd2031 (2006).

[21] Carr, J. A. et al. A microfluidic platform for high-sensitivity, real-time drug screening on C. elegans and parasitic nematodes. Lab on a chip 11, 2385-2396, doi:10.1039/c1lc20170k (2011).

[22] Kopito, R. B. & Levine, E. Durable spatiotemporal surveillance of Caenorhabditis elegans response to environmental cues. Lab on a chip 14, 764-770, doi:10.1039/c3lc51061a (2014).

[23] Leung, C. K., Deonarine, A., Strange, K. & Choe, K. P. High-throughput screening and biosensing with fluorescent C. elegans strains. Journal of visualized experiments : JoVE, doi:10.3791/2745 (2011).

[24] Lehner, B., Tischler, J. & Fraser, A. G. RNAi screens in Caenorhabditis elegans in a 96-well liquid format and their application to the systematic identification of genetic interactions. Nature protocols 1, 1617-1620, doi:10.1038/nprot.2006.245 (2006).

[25] Leung, C. K. et al. An ultra high-throughput, whole-animal screen for small molecule modulators of a specific genetic pathway in Caenorhabditis elegans. PloS one 8, e62166, doi:10.1371/journal.pone.0062166 (2013).

[26] Crisp, Ashley et al. C. elegans model of patterned neurodegeneration induced by APP for high-throughput drug screening. Alzheimer's & Dementia: The Journal of the Alzheimer's Association, Volume 8 , Issue 4 , P307 (2012)

[27] Ghorashian, N., "Automated, microfluidic platforms to facilitate nerve degeneration studies with C. elegans," Doctoral Dissertation, The University of Texas (2013).

[28] Brenner, S. The genetics of Caenorhabditis elegans. Genetics 77, 71-94 (1974).

[29] Kirby B (2010) Micro- and Nanoscale Fluid Mechanics: Transport in Microfluidic Devices. NewYork, NY: Cambridge University Press.

[30] Nguyen NT, Wereley ST (2002) Fundamentals and Applications of Microfluidics. Boston, MA: Artech House. pp. 35-37.

[31] Lee PJ, Ghorashian N, Gaige TA, Hung PJ (2007) Microfluidic system for automated cell-based assays. JALA Charlottesv Va 12:363-367.

[32] Conant CG, Schwartz MA, Beecher JE, Rudoff RC, Ionescu-Zanetti C, Nevill JT (2011) Well plate microfluidic system for investigation of dynamic platelet behavior under variable shear loads. Biotechnol Bioeng. 108: 2978-87.

Vita

Evan Marley Hegarty was born in October of 1983, on The Farm, near Summertown, TN. He was raised in southern Germany, in the state of Bavaria (Bayern Deutschland), where his mom was a teacher and his dad was a carpenter. Evan attended Bamberg High School in Bamberg, Germany and graduated in 2002. Then he pursued a degree in both music and engineering in Gainesville, Florida. After years of this dual study and touring with international artists, Evan ultimately finished his B.S in Mechanical Engineering from The University of Florida in 2011. While participating in IPPD (Integrated Product and Process Design) program at UF, he worked in Dr. Hahn's Laser Diagnostics Lab, which sparked his interest in lasers and optics. After graduating from UF, he worked as a research assistant in Dr. Mohseni's MAV (Micro Air Vehicle) Wind Tunnel Lab where he developed interests in fluid mechanic studies. These interests led Evan to Dr. Adela Ben-Yakar's Lab while attending grad school at The University of Texas at Austin. Since 2012, Evan has been working in the FemtoLAB under Dr. Ben-Yakar in the Department of Mechanical Engineering, Thermal-Fluid Systems. There he has focused on the development of microfluidic platforms for high-throughput optical interrogation of *Caenorhabditis elegans* for large-scale drug screens relating to ageing, Alzheimer's disease, Huntington's disease, and other neurodegenerative disorders.

evanhegarty@gmail.com

This thesis was typed by Evan Marley Hegarty